Università degli Studi di Genova

Scuola Politecnica

Corso di Laurea Magistrale in Ingegneria Meccanica Aeronautica

Analysis of the Forces Acting on Particles in Homogeneous Isotropic Turbulence

—

Tesi di Laurea Magistrale

Relatori:
Prof. J.O. PRALITS
Prof. L. BRANDT

Correlatori:
Dr. G. SARDINA
Dr. F. PICANO

Candidato:
STEFANO OLIVIERI

Anno Accademico 2012/2013

Abstract

The present work deals with particle laden-flows and with small spherical particles dispersed in homogeneous isotropic turbulence, in particular. A one-way coupling is assumed, i.e. the flow acts on particles but not vice versa. The governing mathematical model for this framework features many forces acting on particles, whose evaluation presents several issues so that some strong simplifications are often done. In this work we implement a proper numerical method in order to perform Direct Numerical Simulations with a complete evaluation of all the forces. Afterwards we perform a parametric investigation over a wide range of the particle-to-fluid density ratio and particle response time i.e. Stokes number. Results show how the contributions of the different forces and the preferential accumulation highly vary depending on the values of these parameters. Furthermore, analyzing the specific role of the Basset History force we want to show that this term, often neglected in previous numerical studies, affects the particle behaviour even at high density ratios. Finally, a further investigation is made on the effect of turbulence on the mean particle settling velocity, for cases representative of oceanic phytoplankton. The effect is found to be almost negligible within this particular range, a result that could represent a useful contribution to the existing debate in marine ecology.

Sommario

L'argomento del presente lavoro riguarda la dettagliata analisi delle forze agenti su particelle disperse in un flusso turbolento omogeneo ed isotropo. Il termine particelle in questo ambito può comprendere particelle solide, gocce o bolle, di dimensione inferiore alla più piccola scala caratteristica del flusso. Il problema teorico si correla ad applicazioni di forte interesse quali sistemi combustivi, tecniche di misura fluidodinamiche che fanno uso di traccianti, processi meteorologici e lo studio di microrganismi nell'ecologia marina.

La fase fluida è assunta come un mezzo continuo e studiata con approccio Euleriano mentre le particelle disperse vengono analizzate in chiave Lagrangiana. L'accoppiamento considerato, concordamente ad altri autori, è di tipo *one-way*, cioè il flusso non è modificato dalla presenza delle particelle. Sotto tali ipotesi, la dinamica della particella è governata dal modello matematico di Maxey-Riley.

Il primo punto di particolare interesse che muove il lavoro è la messa a punto di una procedura di calcolo numerico in grado di valutare tutti i termini del modello, cioé tutte le forze agenti sulla particella, che spesso vengono invece trascurati per semplificare l'aspetto teorico ed abbassare l'alto costo computazionale richiesto. La situazione è particolarmente complessa nel caso turbolento, come è noto. A questo proposito, la scelta del modello di turbolenza omogenea isotropa, risolto numericamente tramite metodo pseudospettrale su un dominio triperiodico, è giustificata dall'interesse per processi alle piccole scale.

Tra le varie forze, la cosiddetta *Basset History force* è quella che presenta le difficoltà matematiche maggiori, sia dal punto di vista analitico che numerico. Viene pertanto implementato e testato un metodo per la valutazione di tale termine recentemente pubblicato in letteratura, per poi illustrare lo schema

numerico completo per l'evoluzione delle particelle. Sono presentati diversi test di validazione, tra cui il caso classico della particella sferica in caduta libera in un fluido in quiete.

Il codice sviluppato viene quindi inizialmente utilizzato per effettuare un'indagine parametrica su un ampio spettro di rapporti di densità e numeri di Stokes, parametri che condizionano fortemente la dinamica, al fine di ottenere una classificazione sistematica dei contributi delle differenti forze. Tali contributi sono sinteticamente quantificati dalle *probability density function* del rapporto tra ciascun termine di accelerazione e quella totale. Viene inoltre studiato l'accumulo preferenziale nei diversi casi con visualizzazioni istantanee e soprattutto tramite la *radial distribution function*. I risultati confermano quelli di precedenti lavori mentre alcune interessanti caratteristiche legate all'effetto della forza di Basset vengono messe in evidenza tramite il confronto fra simulazioni con e senza tale termine. Il contributo della forza di Basset risulta quasi sempre non trascurabile ed in particolare troviamo che nel caso di alti rapporti di densità (particelle cosiddette *pesanti*) esso è pari ad un 10% del totale, complementare alla restante *Stokes Drag*, normalmente ritenuta essere l'unico termine rilevante.

Una specifica tematica che viene infine affrontata riguarda l'effetto del flusso turbolento sulla velocità media di sedimentazione delle particelle, in presenza di gravità. L'interesse per tale problema trova fondamento, ad esempio, nello studio di processi ecologici quali la dinamica di microrganismi in ambienti acquatici, con un acceso dibattito tra i ricercatori vista la difficoltà nelle misurazioni e la complessità del fenomeno. La velocità media di sedimentazione che troviamo dalle nostre simulazioni ha una variazione trascurabile rispetto alla velocità terminale a cui tende la particella nel caso di fluido in quiete: l'effetto della turbolenza sulla sedimentazione di particelle di questo tipo risulta irrilevante. Le particelle si comportano praticamente come traccianti e tale risultato è confortato dall'analisi dinamica che risulta molto simile a quanto trovato nell'indagine parametrica per particelle di paragonabile tipologia.

Preface/Prefazione

The present Master's Thesis was developed during a six months visiting period (from September 2012 to March 2013) at *Linné FLOW Centre* (`www.flow.kth.se`), a research center within the *Royal Institute of Technology* (*KTH*) in Stockholm, Sweden, under the supervision of Professor Luca Brandt and Drs. Gaetano Sardina and Francesco Picano.

La presente Tesi di Laurea Magistrale è frutto di un'esperienza semestrale (Settembre 2012 – Marzo 2013) presso il centro di ricerca *Linné FLOW Centre* (`http://www.flow.kth.se`) del *Royal Institute of Technology* (abbr. *KTH*) di Stoccolma (Svezia), sotto la supervisione del Prof. Luca Brandt e dei Dott.ri Gaetano Sardina e Francesco Picano.

Contents

List of Figures

List of Tables

Part I

Introduction and Method

Chapter 1

Introduction

The present work deals with the modelling of *particles*[1] dispersed in turbulent fluid flows, a challenging field for research with applications both in environmental phenomena and industrial processes, such as:

- the motion of plankton, algae and other microorganisms in the ocean;
- rain droplets formation and aerosols dispersion (sand, pollen, pollutants) in the atmosphere;
- the behaviour of particles used as tracers for experimental measurement techniques;
- the dynamics of fuel droplets in combustion systems.

All these applications belong to the family of *particle-laden flows*, which are part of multiphase fluid dynamics. There are many interesting topics related with this framework, even for fundamental research. Among these, it is interesting to identify the role of the different forces acting on particles. The purpose of this work is to give a contribution to this topic.

[1] The word "particles" is general and it is used to denote both solid particles, bubbles and droplets.

(a) *Droplets in clouds*

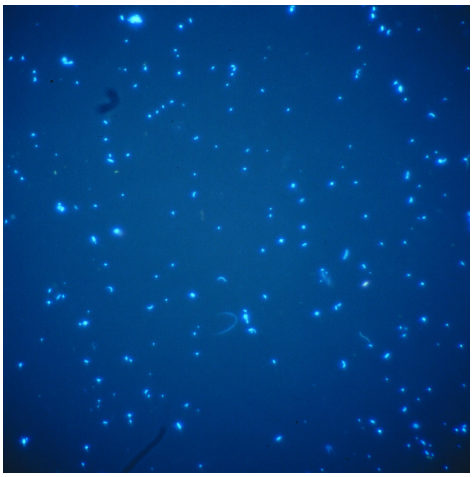

(b) *Microorganisms in the ocean*

Figure 1.1: *Examples of particle-laden flows in nature.*

1.1 Basic features of particle-laden flows

We start by briefly mentioning some important concepts to introduce the reader to the framework of particle-laden flows. Exhaustive presentations can be found in literature [20, 25].

The first essential definition concerns the different components of the system we want to model. The fluid flow, conceived as usual like a *continuum*, will be indicated as the *carrier phase*. Particles, on the other hand, are represented by an ensemble of discrete point-like bodies; they will be denoted as the *dispersed phase*. The densities of the carrier and dispersed phase are generally different and particles are small but have finite dimension. It is evident that a major difference exists between these two phases; that's why they will be studied with totally different approaches.

1.1.1 Dilution

An essential point in the analysis of particle-laden flows is the description and understanding of the dilution level of the dispersed phase. A measure can be given by the *volume fraction* and the *mass loading*. However, because of complicated effects such as the formation of particle clusters that are responsible of locally

nonuniform concentrations, a rigorous description of the dilution level is not so obvious [20].

1.1.2 Coupling

An interesting aspect concerns the flow modification due to the presence of particles. We briefly present the possible situations and approaches in this regard:

- for adequately small particles and dilute conditions the carrier phase is usually thought not to be modified by particle presence (*one-way coupling*);
- in the *two-way coupling* approach the countereffect on the carrier flow is taken into account. According to this approach flow stability and turbulence modifications induced by the interaction with dispersed particles are frequently investigated;
- finally, in the *four-way coupling* mutual interactions between different particles are also taken into account. This approach is interesting for the so-called dense suspensions.

Different methods of analysis are used depending on the coupling effects we consider. In the present work we will use a one-way coupling approach, since it is consistent with our purposes.

1.2 Assumptions on particles

In the present work the following assumptions are made:

- particles are assumed to be *spherical*[2];
- particles are assumed to be *small* compared to the smallest flow scales[3];
- a *one-way coupling* configuration is assumed.

These assumptions are determinant for the mathematical model to be used and are representative of an interesting branch of research.

[2]No variations in the shape or volume are allowed.
[3]We will rigorously define this condition later.

1.3 Literature review

Before proceeding further, we recall hereunder the most important results in the reference literature to provide an overall picture and a framework for our contribution.

The derivation of the governing model for the motion of a sphere immersed in a flow comes from a long path. The works by Basset, Boussinesq and Oseen [7, 9, 26] describing the dynamics of a sphere falling in a quiescent fluid are early and well-known studies. Efforts were made to extend these results to nonuniform and unsteady flows [37, 11, 33]; finally Maxey and Riley [23] proposed a formulation that has been widely accepted and used since then[4]. An essential fact is that the resulting governing model features many forces acting on the particle, and computational difficulties arise when considering the complete form that accounts for all the terms.

In the matter of applications, many works examined the distribution of the dispersed phase in space, especially for the case of turbulent flows. Earlier contributions include experiments [35], analytical studies [30, 31, 24] and numerical simulations [36, 13]. The relevant insight was that particles showed dispersion properties different from fluid elements. Unlike an uniform distribution, the formation of clusters in certain regions of the flow was observed. This behavior takes the name of *preferential accumulation* and appears to be really an intriguing feature.

Another topic of interest concerns the settling of particles under the effect of gravity and the effect of turbulence on the mean sedimentation rate of particles. This problem has been studied numerically for different flow types, including rotating cells [22], gaussian random fields [21] and homogeneous isotropic turbulence [39]; the latter work showed a remarkable increase of the settling velocity of heavy particles with respect to the particle terminal velocity in still fluid.

All the works cited so far neglected some of the forces acting on particles. This could have been done since particles much heavier than the fluid were considered; in this limit situations, some approximations appear to be justified. On the other hand, in the investigation of particle-to-fluid density ratios of $\mathcal{O}(1 \div 10)$ all the

[4] An historical review about the derivation of the model can be found in [25].

forces are to be taken into account.

Methods and computational resources for the evaluation of the complete dynamics are becoming available only recently. Results of this kind include the analysis of the role of the different forces for turbulent channel flow [4] and the quantification of the dispersion properties of particles in stratified turbulence [2, 1]. The present work deals with these latter issues, with a particular focus that will be explained in the following sections.

1.4 Homogeneous isotropic turbulence

Our aim is to present a contribution which can be useful for many situations and in a general sense. As we have already stated, encountered fluid flows are very often in a turbulent condition. In fact, it is an intrinsic behaviour predicted by the governing equations for fluid motions. Essential features of turbulence are the apparently random behaviour and the wide spectrum of scales. The flow setting chosen for our investigation is *homogeneous isotropic turbulence*. This is done for several reasons:

- it is an ideal but quite general scenario, hence it has importance on the theoretical side and it is frequently adopted in fundamental research;
- it represents a valid framework for investigating small-scale phenomena like the interaction between particles and the surrounding flow.

We briefly recall some basic features of this model. Further information can be found in exhaustive textbooks [15, 27]. An unbounded tridimensional space, without solid boundaries, is considered; this situation can be reproduced choosing a cubic domain of side $\mathcal{L}$ with periodic boundary conditions. The peculiar feature is that the statistical properties do not depend on position and time (homogeneity) and on the chosen frame of reference (isotropy). The mean flow velocity is consequently zero, together with many averaged quantities. Even if the assumptions can hold strictly only for an ideal configuration, this can be a first approximation for many situations.

1.5 Main issues on particle dynamics

The dynamics of a spherical particle, immersed in a nonuniform unsteady flow, is known to be ruled by the presence of many forces. Using the second law of motion, we can write [23]:

$$m_{\mathrm{p}} \frac{\mathrm{d}\mathbf{V}}{\mathrm{d}t} = \mathbf{F}_{\mathrm{SD}} + \mathbf{F}_{\mathrm{PG}} + \mathbf{F}_{\mathrm{AM}} + \mathbf{F}_{\mathrm{Gr}} + \mathbf{F}_{\mathrm{Ba}} \tag{1.1}$$

where m_{p} and $\mathbf{V}$ are respectively the mass and the velocity of the particle. At the right-hand side we have the forces, respectively known as: *Stokes Drag*, *Pressure Gradient*, *Added Mass*, *Gravity* and *Basset History force*[5].

In the existing numerical investigations, some of the forces are often neglected. This can be done for two reasons. The first is a reasoned approximation based on the value of some parameters, such as the ratio between the densities of the two phases; for much heavier-than-fluid particles, as an example, the governing equation could actually be approximated to a form in which only the Stokes drag and gravity are non-negligible quantities. However, this assumption can be done only for high density ratios.

The second point is represented by the difficulty of computing each of the forces, especially the Basset History force. Without going into details for now, we only mention its dependence from all the previous history of the particle, a delicate aspect from the computational point of view. The specific problem of the efficient calculation of the Basset force will therefore need to be analyzed.

The issues just mentioned hold for many flow configurations, including non-turbulent flows. When dealing with turbulence, a further degree of complexity is introduced. Some questions could be outlined in order to introduce the scope of the present work:

- Is the evaluation of all the forces really needed?
- How can we efficiently compute all the forces?
- Which is the contribution from each force?

[5] A discussion of the physical meaning of each force will be given in §2.2.1.

- Are there some characteristic parameters that dramatically affect the dynamics of particles?

We aim to face these questions and to give some interesting answers. The following paragraph explains the main points and goals of the activity that has been carried out.

1.6 Scope and structure of the work

The main goal of the present work is to investigate the role of all the known forces acting on small spherical particles dispersed in homogeneous isotropic turbulence. Investigations are performed by means of *Direct Numerical Simulations*. After the implementation of a proper numerical method that accounts for all the forces acting on particles, simulations are performed in order to investigate parametrically the role of the different forces for different types of particles. Statistical results are elaborated in order to show the prevailing forces and the major insights are discussed. As a further interesting case of application, we will later investigate the effect of turbulence on the mean settling velocity of nearly neutrally-buoyant particles, a representative case for microorganisms in the ocean. Contents of the present document are organized as follows:

- the present chapter is an introduction of the problem;
- Chapter 2 explains the assumed mathematical model, presents the governing equations and discusses the physical meaning;
- Chapter 3 describes the adopted numerical method and its peculiar features;
- Chapter 4 gives general informations on the performed simulations;
- Chapter 5 presents the results of the parametric investigation;
- Chapter 6 deals with the sedimentation of slightly heavier-than-fluid particles;
- conclusions and outlook are finally discussed in Chapter 7.

Chapter 2

Mathematical Model

This chapter presents the mathematical model with the governing equations. Moreover, some important concepts of physical significance are discussed.

Several approaches have been developed for the analysis of particle-laden flows [6]. The present one can be defined as *Eulerian-Lagrangian* because of the respective ways of analysis adopted for the fluid and for the particles. Flow quantities are described as fields, the fluid velocity field is therefore written as $\mathbf{u} = \mathbf{u}(\mathbf{x}, t)$. The motion of particles, on the other hand, is investigated following the material particle: $\mathbf{X} = \mathbf{X}(t)$. We notice the fundamental main difference: $\mathbf{x}$ is an indipendent position in the domain, $\mathbf{X}(t)$ is the position assumed by a particle at the time t.

2.1 Carrier flow

The fluid flow dynamics is governed by the incompressible Navier-Stokes equations, respectively describing the conservation of mass and momentum:

$$\nabla \cdot \mathbf{u} = 0 \tag{2.1}$$

$$\frac{\partial \mathbf{u}}{\partial t} + \mathbf{u} \cdot \nabla \mathbf{u} = -\frac{1}{\rho_\mathrm{f}} \nabla p + \nu \nabla^2 \mathbf{u} + \mathbf{f} \tag{2.2}$$

where $\mathbf{u}(\mathbf{x}, t)$ is the fluid velocity field, ρ_f is the fluid density, $p(\mathbf{x}, t)$ is the pressure field, ν is the fluid kinematic viscosity, $\mathbf{f}(\mathbf{x}, t)$ is the external forcing field. The

assumed domain is a cube of side $\mathcal{L}$ with periodic boundary conditions. The external forcing has a given law and its presence is essential in order to assure the development of statistical stationarity.

One major concept of turbulent flows is certainly the energy cascade. The energy injected at the large scales is transported through a continuous range of scales (the *inertial subrange*) until a finite limit where the viscosity acts to dissipate energy. The smallest scale is known as the *Kolmogorov microscale* (usually denoted with η or "K"). Its average values are found with dimensional arguments [27]:

$$\eta = \left(\frac{\nu^3}{\epsilon}\right)^{\frac{1}{4}} \tag{2.3}$$

$$u_{\mathrm{K}} = (\epsilon\,\nu)^{\frac{1}{4}} \tag{2.4}$$

$$\tau_{\mathrm{K}} = \left(\frac{\nu}{\epsilon}\right)^{\frac{1}{2}} \tag{2.5}$$

where η, u_{K}, τ_{K} are respectively the length, velocity and time of the the Kolmogorov scale, ϵ is the mean energy dissipation rate of the flow and ν is the fluid viscosity.

Using dimensional arguments, an important prediction on the energy spectrum $E(k)$ (where $k = 2\pi/\lambda$ is the wave number) can be found:

$$E(k) \sim k^{-\frac{5}{3}} \tag{2.6}$$

which gives an important insight on the energy distribution over the range of scales of the flow motion and finds a good agreement with experimental verifications. We can see the characteristic form in Fig. 2.1, where we report the averaged flow energy spectrum from our code.

2.2 Particle dynamics

The study of the dispersed phase is done through a Lagrangian description: each of the N_{p} particles initially released into the flow is tracked by evaluating the

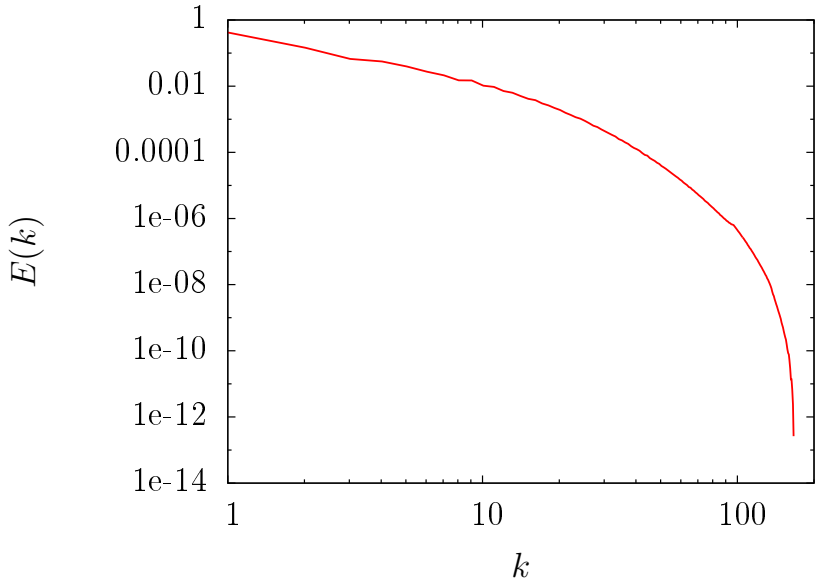

Figure 2.1: *Averaged flow energy spectrum for the performed simulations as a function of the wavenumber k.*

position of its center at a certain time, $\mathbf{X}(t)$, from:

$$\frac{\mathrm{d}\mathbf{X}}{\mathrm{d}t} = \mathbf{V}(t) \tag{2.7}$$

The particle velocity is generally different from that of the surrounding fluid and obeys to the following equation:

$$\begin{aligned} m_\mathrm{p}\frac{\mathrm{d}\mathbf{V}}{\mathrm{d}t} = 6\pi r_\mathrm{p}\mu[\mathbf{u}(\mathbf{X}(t),t) - \mathbf{V}(t) + \frac{1}{6}r_\mathrm{p}^2\nabla^2\mathbf{u}|_{\mathbf{X}(t)}] + m_\mathrm{f}\left.\frac{\mathrm{D}\mathbf{u}}{\mathrm{D}t}\right|_{\mathbf{X}(t)} + (m_\mathrm{p} - m_\mathrm{f})\mathbf{g} + \\ + \frac{1}{2}m_\mathrm{f}\left[\left.\frac{\mathrm{D}\mathbf{u}}{\mathrm{D}t}\right|_{\mathbf{X}(t)} - \frac{\mathrm{d}\mathbf{V}}{\mathrm{d}t} + \frac{1}{10}r_\mathrm{p}^2\frac{\mathrm{d}}{\mathrm{d}t}(\nabla^2\mathbf{u})\right|_{\mathbf{X}(t)}\right] + \\ + 6r_\mathrm{p}^2\rho_\mathrm{f}\sqrt{\pi\nu}\int_0^t \frac{1}{\sqrt{t-\tau}}\frac{\mathrm{d}}{\mathrm{d}\tau}[\mathbf{u}(\mathbf{X}(t),t) - \mathbf{V}(t) + \frac{1}{6}r_\mathrm{p}^2\nabla^2\mathbf{u}|_{\mathbf{X}(t)}]\,\mathrm{d}\tau \end{aligned} \tag{2.8}$$

which is historically known as the Basset-Boussinesq-Oseen equation. The most general form was derived by M. R. Maxey and J. J. Riley in 1983, hence it is also called as the *Maxey-Riley equation* [23]. Here, $\mathbf{u}(\mathbf{X}(t),t)$ is the flow velocity

sampled at the particle position, ρ_f is the fluid density, ρ_p is the particle density, r_p is the particle radius, μ and ν are respectively the dynamic and kinematic viscosities of the fluid, $m_\mathrm{p} = \frac{4}{3}\pi r_\mathrm{p}^3 \rho_\mathrm{p}$ is the particle mass, $m_\mathrm{f} = \frac{4}{3}\pi r_\mathrm{p}^3 \rho_\mathrm{f}$ is the mass of the fluid element of same volume and $\mathbf{g}$ is the gravitational acceleration vector.

Eq. (2.8) holds strictly for small spherical rigid particles in nonuniform and unsteady flows, under the following conditions:

$$\frac{r_\mathrm{p}}{\eta} \ll 1 \tag{2.9}$$

$$Re_\mathrm{p} = \frac{r_\mathrm{p}|V_0 - U_0|}{\nu} \ll 1 \tag{2.10}$$

where η is the Kolmogorov length scale, V_0 and U_0 are representative magnitudes of the particle velocity and the surrounding fluid, respectively. Eq. (2.9) means that the particle needs to be much smaller than the smallest flow structure while (2.10) means that the particle has to experience a creeping flow i.e. a flow governed by viscous forces [25].

An important remark has to be done regarding the different material derivatives which are involved: $\frac{\mathrm{d}}{\mathrm{d}t}$ means the Lagrangian derivative following the solid particle while $\frac{\mathrm{D}}{\mathrm{D}t}$ the Lagrangian derivative following the fluid particle. Hence:
$\frac{\mathrm{d}(\cdot)}{\mathrm{d}t} = \frac{\partial(\cdot)}{\partial t} + \mathbf{V}\cdot\nabla(\cdot)$ and $\frac{\mathrm{D}(\cdot)}{\mathrm{D}t} = \frac{\partial(\cdot)}{\partial t} + \mathbf{u}\cdot\nabla(\cdot)$. We can relate the two quantities:

$$\frac{\mathrm{D}(\cdot)}{\mathrm{D}t} = \frac{\mathrm{d}(\cdot)}{\mathrm{d}t} - \mathbf{w}\cdot\nabla(\cdot) \tag{2.11}$$

where $\mathbf{w} = (\mathbf{V} - \mathbf{u})$ is the relative velocity of the particle with respect to the flow.

In (2.8) the correction terms for finite size effects are shown; in the following they will be neglected since particles are assumed to be sufficiently small.

2.2.1 Forces description

The Maxey-Riley equation expresses the second law of motion, with the different forces on particles appearing at the right-hand-side:

$$m_{\mathrm{p}}\frac{\mathrm{d}\mathbf{V}}{\mathrm{d}t} = \overbrace{6\pi r_{\mathrm{p}}\mu[\mathbf{u}(\mathbf{X}(t),t)-\mathbf{V}(t)]}^{\mathbf{F}_{\mathrm{SD}}} + \overbrace{m_{\mathrm{f}}\frac{\mathrm{D}\mathbf{u}}{\mathrm{D}t}\bigg|_{\mathbf{X}(t)}}^{\mathbf{F}_{\mathrm{PG}}} + \overbrace{(m_{\mathrm{p}}-m_{\mathrm{f}})\mathbf{g}}^{\mathbf{F}_{\mathrm{Gr}}} + \\ + \underbrace{\frac{1}{2}m_{\mathrm{f}}\left[\frac{\mathrm{D}\mathbf{u}}{\mathrm{D}t}\bigg|_{\mathbf{X}(t)} - \frac{\mathrm{d}\mathbf{V}}{\mathrm{d}t}\right]}_{\mathbf{F}_{\mathrm{AM}}} + \underbrace{6r_{\mathrm{p}}^2\rho_{\mathrm{f}}\sqrt{\pi\nu}\int_0^t \frac{1}{\sqrt{t-\tau}}\frac{\mathrm{d}}{\mathrm{d}\tau}[\mathbf{u}(\mathbf{X}(t),t)-\mathbf{V}(t)]\,\mathrm{d}\tau}_{\mathbf{F}_{\mathrm{Ba}}} \tag{2.12}$$

$$= \mathbf{F}_{\mathrm{SD}} + \mathbf{F}_{\mathrm{PG}} + \mathbf{F}_{\mathrm{AM}} + \mathbf{F}_{\mathrm{Gr}} + \mathbf{F}_{\mathrm{Ba}}$$

The forces respectively take the following names: Stokes Drag, Pressure Gradient, Added Mass, Gravity and Basset History force. We hereunder briefly discuss each of these terms.

The first term models the friction exerted on the particle due to viscosity. It is useful to think at the case of a settling sphere in a quiescent fluid. The famous result from G. G. Stokes (1851) is that the sphere asymptotically reaches a *terminal velocity* that is expressed as $V_{\mathrm{T}} = \frac{2}{9}r_{\mathrm{p}}^2\frac{\rho_{\mathrm{p}}-\rho_{\mathrm{f}}}{\mu}g$. Gravity is balanced by the viscous force equal to $F_{\mathrm{SD}} = 6\pi\mu r_{\mathrm{p}}V_{\mathrm{T}}$.

The second term is usually called as the Pressure Gradient force and represents the force at which a sphere of fluid with the same volume of the particle is subjected in the undisturbed flow. The present form was derived by Riley [33].

Gravity is a well-known, constant volume force acting on bodies. We note that the buoyancy effect is also taken into account within the equation.

The Added Mass effect is due to the fact that the particle displaces the fluid during its motion. Usually this term is modelled by considering an additional fluid mass moving together with the object. For a spherical object, this is found to be half of its mass. Also for the added mass, several derivations have been presented, starting from the first studies by Bessel in 1828 to the form proposed by Auton [5], which is widely accepted and used in the most recent studies.

Finally, the Basset History force is perhaps the less known term; it models unsteady viscous effects such as the transient development of the boundary layer. Its analytical expression was derived indipendently by Boussinesq in 1885 and Basset in 1888 [9, 7]. The Basset force has an integral form, which involves the previous time instants. Its computation is both theoretically and numerically hard to deal with, that's why this term is often neglected; however it can be relevant in some cases such as highly accelerated creeping flows.

2.2.2 Rearrangement and nondimensionalization

Dividing (2.12) by $m_\mathrm{p} = \frac{4}{3}\rho_\mathrm{p}\pi {r_\mathrm{p}}^3$ and after some manipulations, one finds the Maxey-Riley equation written in terms of accelerations, instead of forces:

$$\frac{\mathrm{d}\mathbf{V}}{\mathrm{d}t} = \frac{1}{\tau_\mathrm{p}}(\mathbf{u}-\mathbf{V}) + \frac{\rho_\mathrm{f}}{\rho_\mathrm{p}}\frac{\mathrm{D}\mathbf{u}}{\mathrm{D}t} + (1-\frac{\rho_\mathrm{f}}{\rho_\mathrm{p}})\mathbf{g} + \\ + \frac{1}{2}\frac{\rho_\mathrm{f}}{\rho_\mathrm{p}}(\frac{\mathrm{D}\mathbf{u}}{\mathrm{D}t} - \frac{\mathrm{d}\mathbf{V}}{\mathrm{d}t}) + \sqrt{\frac{9}{2\pi}\frac{\rho_\mathrm{f}}{\rho_\mathrm{p}}\frac{1}{\tau_\mathrm{p}}}\int_0^t \frac{1}{\sqrt{t-\tau}}\frac{\mathrm{d}}{\mathrm{d}\tau}(\mathbf{u}-\mathbf{V})\,\mathrm{d}\tau \quad (2.13)$$

where we have defined the particle *response time*:

$$\tau_\mathrm{p} = \frac{2}{9}\frac{r_\mathrm{p}^2}{\nu}\frac{\rho_\mathrm{p}}{\rho_\mathrm{f}} \quad (2.14)$$

which is an important parameter measuring the inertia of the particle. In the limit of $\tau_\mathrm{p} \to 0$ the point-like particle follows exactly the flow i.e. it is a perfect *tracer*.

As a next step, we can scale with a general set of reference quantities L_ref, t_ref,V_ref in order to obtain a dimensionless form of the equation. We further define:

$$St = \frac{\tau_\mathrm{p}}{t_\mathrm{ref}} \quad (2.15)$$

$$Fr = \frac{V_\mathrm{ref}/t_\mathrm{ref}}{g} \quad (2.16)$$

which are respectively the *Stokes* and *Froude* dimensionless numbers. The resulting

equation is:

$$\frac{\mathrm{d}\mathbf{V}}{\mathrm{d}t} = \frac{1}{St}(\mathbf{u}-\mathbf{V}) + \rho\frac{\mathrm{D}\mathbf{u}}{\mathrm{D}t} + \frac{(1-\rho)}{Fr}\mathbf{e}_g + \\ + \frac{1}{2}\rho(\frac{\mathrm{D}\mathbf{u}}{\mathrm{D}t} - \frac{\mathrm{d}\mathbf{V}}{\mathrm{d}t}) + \sqrt{\frac{9}{2\pi}\frac{\rho}{St}}\int_0^t \frac{1}{\sqrt{t-\tau}}\frac{\mathrm{d}}{\mathrm{d}\tau}(\mathbf{u}-\mathbf{V})\,\mathrm{d}\tau \quad (2.17)$$

where $\mathbf{e}_g$ is the unit vector parallel to the gravity direction and $\rho = \rho_\mathrm{f}/\rho_\mathrm{p}$.

In the context of small particles in turbulent flows, the Stokes number is usually defined using the Kolmogorov time scale:

$$St_\mathrm{K} = \frac{\tau_\mathrm{p}}{\tau_\mathrm{K}} \quad (2.18)$$

2.2.3 Limit cases

We stated in the introduction that this work aims to solve the full equation governing the particle dynamics. However, there are some situations in which the Maxey-Riley equation could be reasonably simplified. We briefly explain these cases. This will also be useful when discussing our results.

The first situation is to consider high density ratios ($\rho_\mathrm{p}/\rho_\mathrm{f} \gg 1$). Due to this assumption, by neglecting all the terms divided by the density ratio, (2.13) has been often approximated by [39]:

$$\frac{\mathrm{d}\mathbf{V}}{\mathrm{d}t} = \frac{1}{\tau_\mathrm{p}}(\mathbf{u}-\mathbf{V}) + \mathbf{g} \quad (2.19)$$

This is the case of the so-called *heavy* particles, which is suitable for example in the modelling of aerosol particles. Due to the strong mathematical simplifications, this regime could have been deeply investigated and several important results were found (see §1.3).

Another situation that is useful to compare with is the Lagrangian description of the fluid particle, an important topic of one-phase fluid mechanics and mixing [38, 18]. It is known that the relative mathematical description comes from:

$$\frac{\mathrm{d}\mathbf{X}}{\mathrm{d}t} = \mathbf{u}(t) \quad (2.20)$$

which rigorously describes the motion of a fluid element, but can also be assumed as a valid approximation for tracer-like particles. Several experimental techniques are based on the use of particles that *trace* the fluid flow [3], behaving approximately like fluid elements do. The Stokes number here represents the control parameter and has to be taken as low as possible.

Both above identified limit cases and some intermediate conditions will be investigated in the following chapters.

Chapter 3

Numerical Method

Two elements clearly indicate the need of numerical simulations. First, we deal with the Navier-Stokes equations and turbulent flows, the complexity of which is well-known. On the other hand, it has been shown that the governing equation for the motion of particles is also complicated. Theoretical studies of the Maxey-Riley equation are an interesting and active subject but no general solution has been found until now. Hence the adopted strategy for this investigation will be of computational nature. In the following the chosen numerical method will be explained.

3.1 Overall description

The flow is solved with the so-called *pseudospectral method*, writing the solution as a finite Fourier series. Trasformations between real and Fourier spaces are involved. High accuracy is reached with this kind of approach, the resolution being related with the number of considered modes.

The particle velocity and trajectory are evolved at each time step by discretizing the governing equations. Flow quantities are evaluated at the nodes of a regular grid while the particle can be located anywhere, thus a quadratic interpolation is performed.

As a particular issue inside the particle evolution we mention the computation of the Basset history term, which is the integral term that appears in the Maxey-

Riley equation; we present the implementation of a recently developed method to reach good computational efficiency and accuracy.

3.2 Pseudospectral flow solver

The present investigation is done by means of Direct Numerical Simulations i.e. the Navier-Stokes equations are fully solved at all scales of motion. This is frequently achieved by applying the so-called *pseudospectral method*. In the following the basis of this kind of solver are recalled. Further resources can be found in [27].

Spectral methods are characterized by the fact that computations are not made in the real space but in a spectral one using Fourier transform. This is an interesting choice in fluid dynamics since the Fourier transformed form of the Navier-Stokes equations no longer involves derivatives in space, but only in time. However, problems could arise from the computation of the nonlinear terms in the equation, which should be done through a convolution integral. This weighty operation is normally avoided with an inverse transformation back to the real space. This particular procedure takes the name of pseudospectral method.

The velocity field is written as a Fourier series:

$$\mathbf{u}(\mathbf{x},t) = \sum_{\mathbf{k}} e^{i\mathbf{k}\cdot\mathbf{x}}\hat{\mathbf{u}}(\mathbf{k},t) \tag{3.1}$$

where $\mathbf{k}$ is the wavenumber vector, $\hat{\mathbf{u}}(\mathbf{k},t)$ is the Fourier coefficient and use of the complex exponential function is made. The generic wavenumber can be expressed as:

$$\mathbf{k} = k_0\mathbf{n} = k_0(\mathbf{e}_1 n_1 + \mathbf{e}_2 n_2 + \mathbf{e}_3 n_3) \tag{3.2}$$

with $1 - N/2 < n_i < N/2$ and $k_0 = 2\pi/\mathcal{L}$ ($\mathcal{L}$ is the side of the cubical simulation domain). The integer N indicates the range of considered modes and, at the same time, determines the grid resolution. In fact, the latter is related with the highest wavenumber that is considered:

$$\Delta x = \frac{\mathcal{L}}{N} = \frac{\pi}{k_{\max}} \tag{3.3}$$

where $k_{\max} = \frac{1}{2}Nk_0 = \frac{\pi N}{\mathcal{L}}$.

When dealing with the discretized form, trasformations between the real and the Fourier space are operated by the *Fast Fourier Transform*. Due to the finite number of modes taken into account, an adequate dealiasing processing has to be applied. Finally, in the present code advancement in time is performed with a low-storage third-order Runge-Kutta algorithm where the time step is determined by the CFL stability condition.

3.3 Particle tracking

3.3.1 Basset force computation

Before we present how the particle tracking is performed numerically, focus has to be made on a particular component. When solving the Maxey-Riley equation, in fact, a challenging issue comes out with the computation of the Basset History force:

$$\mathbf{F}_{\mathrm{Ba}}(t) = 6r_{\mathrm{p}}^2\rho_{\mathrm{f}}\sqrt{\pi\nu}\int_0^t \frac{1}{\sqrt{t-\tau}}\frac{\mathrm{d}}{\mathrm{d}\tau}[\mathbf{u}(\tau) - \mathbf{V}(\tau)]\mathrm{d}\tau \tag{3.4}$$

Theoretically, at each time step an integral over the whole velocity history of each particle should be performed, this resulting in high computational cost. In many studies the Basset force has been neglected. Other situations show however the peculiar importance of this kind of force [4, 24]. In the present work, the role the Basset force is one of the major targets of investigation.

For our computations, we chose to use the method recently developed by Hinsberg *et al.* in [16]. In the following the method will be briefly explained and results of performed validations will be shown.

Method

We rewrite (3.4) in a more compact form:

$$\mathbf{F}_{\mathrm{Ba}}(t) = C_{\mathrm{Ba}}\int_0^t K_{\mathrm{Ba}}(t-\tau)\mathbf{g}(\tau)\,\mathrm{d}\tau \tag{3.5}$$

where $C_{\mathrm{Ba}} = 6r_{\mathrm{p}}^2\rho_{\mathrm{f}}\sqrt{\pi\nu}$, $K_{\mathrm{Ba}}(t-\tau) = \frac{1}{\sqrt{t-\tau}}$, and $\mathbf{g}(\tau) = \frac{\mathrm{d}}{\mathrm{d}\tau}(\mathbf{u}-\mathbf{V})$. It is important to notice the singularity of the kernel function $K_{\mathrm{Ba}}(t-\tau)$ for $\tau = t$, a delicate issue in the development of methods for computing the Basset term. The computation of $\mathbf{F}_{\mathrm{Ba}}$ is done by splitting the integral into two parts, which will be denoted respectively as the *window* and the *tail*:

$$\mathbf{F}_{\mathrm{Ba}}(t) = C_{\mathrm{Ba}} \int_0^{t-t_{\mathrm{win}}} K_{\mathrm{Ba}}(t-\tau)\mathbf{g}(\tau)\,\mathrm{d}\tau + C_{\mathrm{Ba}} \int_{t-t_{\mathrm{win}}}^{t} K_{\mathrm{Ba}}(t-\tau)\mathbf{g}(\tau)\,\mathrm{d}\tau \tag{3.6}$$

$$\begin{aligned} \mathbf{F}_{\mathrm{Ba,win}}(t) &= C_{\mathrm{Ba}} \int_{t-t_{\mathrm{win}}}^{t} K_{\mathrm{Ba}}(t-\tau)\mathbf{g}(\tau)\,\mathrm{d}\tau \\ \mathbf{F}_{\mathrm{Ba,tail}}(t) &= C_{\mathrm{Ba}} \int_0^{t-t_{\mathrm{win}}} K_{\mathrm{Ba}}(t-\tau)\mathbf{g}(\tau)\,\mathrm{d}\tau \end{aligned} \tag{3.7}$$

$$\mathbf{F}_{\mathrm{Ba}}(t) = \mathbf{F}_{\mathrm{Ba,win}}(t) + \mathbf{F}_{\mathrm{Ba,tail}}(t) \tag{3.8}$$

Numerical integration is performed over the window interval $[t - t_{\mathrm{win}}, t]$ while the approximation of the tail is done by using recursive exponentials, obtaining lower computational cost and higher accuracy with respect to previously developed methods.

The window interval $[t - t_{\mathrm{win}}, t]$ is divided into N_{w} subintervals in order to apply numerical integration. However, the above mentioned singularity does not allow the use of trapezoidal rule on the whole integrand, hence only $\mathbf{g}(\tau)$ is approximated by its linear interpolant, so that:

$$\begin{aligned} \mathbf{F}_{\mathrm{Ba,win}}(t) &= C_{\mathrm{Ba}} \sum_{n=1}^{N_{\mathrm{w}}} \int_{\tau_n}^{\tau_{n-1}} \frac{\mathbf{g}(\tau)}{\sqrt{t-\tau}}\,\mathrm{d}\tau \\ &\approx C_{\mathrm{Ba}} \sum_{n=1}^{N_{\mathrm{w}}} \int_{\tau_n}^{\tau_{n-1}} \frac{\mathbf{g}_n + (\mathbf{g}_{n-1} - \mathbf{g}_n)(\tau - \tau_n)/\Delta t}{\sqrt{t-\tau}}\,\mathrm{d}\tau \end{aligned} \tag{3.9}$$

where $\tau_n = t - n\Delta t$, $n = 0, 1, 2, \ldots, N_{\mathrm{w}}$ and $\Delta t = t_{\mathrm{win}}/N_{\mathrm{w}}$. The latter expression

Table 3.1: *Coefficients for the tail of Basset History term (from Hinsberg et al).*

$\tilde{t}_i$	a_i
0.1	0.23477481312586
0.3	0.28549576238194
1	0.28479416718255
3	0.26149775537574
10	0.32056200511938
40	0.35354490689146
190	0.39635904496921
1000	0.42253908596514
6500	0.48317384225265
50000	0.63661146557001

is then solved exactly, giving:

$$\begin{aligned}\mathbf{F}_{\mathrm{Ba,win}}(t) \approx & \frac{4}{3} C_{\mathrm{Ba}} \sqrt{\Delta t}\, \mathbf{g}_0 + \\ & + \sum_{n=1}^{N_{\mathrm{w}}-1} C_{\mathrm{Ba}} \sqrt{\Delta t} \left[\frac{4}{3}(n-1)\sqrt{n-1} - \frac{8}{3} n \sqrt{n} + \frac{4}{3}(n+1)\sqrt{n+1} \right] \mathbf{g}_n + \\ & + C_{\mathrm{Ba}} \sqrt{\Delta t} \left[\frac{4}{3}(N_{\mathrm{w}}-1)\sqrt{N_{\mathrm{w}}-1} + (2 - \frac{4}{3} N_{\mathrm{w}})\sqrt{N_{\mathrm{w}}} \right] \mathbf{g}_{N_{\mathrm{w}}}\end{aligned} \tag{3.10}$$

A detailed derivation of this result is given in Appendix A.

The tail component is written as a series of exponential functions:

$$\mathbf{F}_{\mathrm{Ba,tail}}(t) = \sum_{i=1}^{m} a_i \mathbf{F}_i(t) \tag{3.11}$$

Each exponential $\mathbf{F}_i$ is composed of a direct and a recursive part, which are expressed as follows:

$$\mathbf{F}_{i,\mathrm{di}} = 2 C_{\mathrm{Ba}} \sqrt{e t_i}\, e^{-\frac{t_{\mathrm{win}}}{2t_i}} \left\{ \left[1 - \phi(-\frac{\Delta t}{2t_i}) \right] \mathbf{g}_{N_{\mathrm{w}}} + e^{-\frac{\Delta t}{2t_i}} \left[\phi(\frac{\Delta t}{2t_i}) - 1 \right] \mathbf{g}_{N_{\mathrm{w}}+1} \right\} \tag{3.12}$$

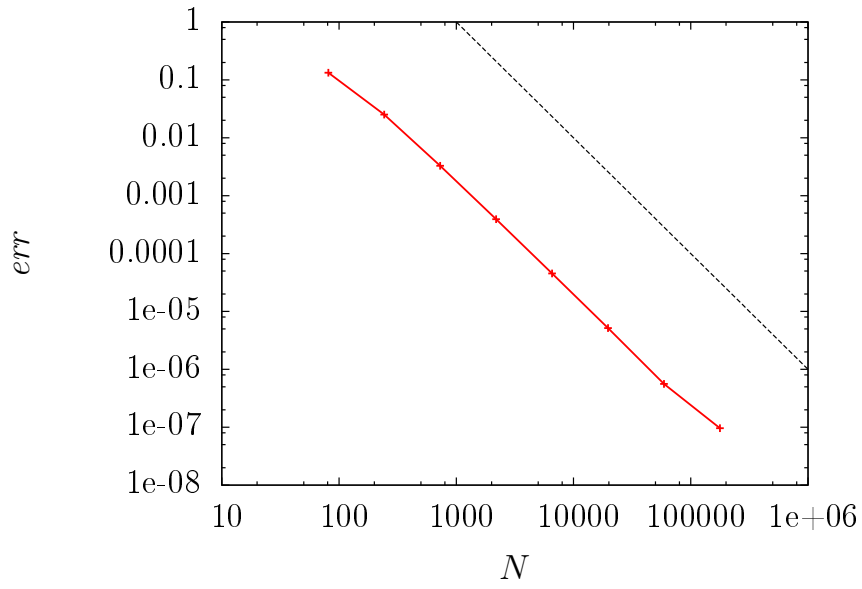

Figure 3.1: *Window-only test. Relative error as a function of the grid resolution (the dashed line represents a second order slope).*

$$\mathbf{F}_{i,\mathrm{re}} = e^{-\frac{\Delta t}{2t_i}}\mathbf{F}_i(t-\Delta t) \tag{3.13}$$

Here, $\phi(z) = \frac{e^z-1}{z}$, $t_i = \tilde{t}_i\, t_{\mathrm{win}}$, a_i and $\tilde{t}_i$ are positive constants found by considerations on the error minimization. The adopted set of values, given by the authors of the method, for the case $m = 10$ is reported in Table 3.1.

Validation

The implementation of the method into our code has been first tested with simple cases, considering only the computation of expression (3.5) separately from the overall scheme.

First we have reproduced the same test in [16], example 1. Here, $g(\tau) = \cos(\tau)$, the chosen time interval is $[0, 50\pi]$ which is discretized using N points. For this case, an exact solution for (3.5) is available from literature:

$$F_{\mathrm{Ba}}(t) = C_{\mathrm{Ba}}\int_0^t K_{\mathrm{Ba}}(t-\tau)\cos(\tau)\,\mathrm{d}\tau = C_{\mathrm{Ba}}\sqrt{2\pi}\Big(C(\sqrt{2t/\pi})\cos t + S(\sqrt{2t/\pi})\sin t\Big) \tag{3.14}$$

where $C(t)$ and $S(t)$ are respectively the Fresnel cosine and sine integral. Fig. 3.1

shows results of calculations considering different N. We found values for the relative error $err = \left|\frac{F_{\mathrm{Ba}} - F_{\mathrm{Ba,ex}}}{F_{\mathrm{Ba,ex}}}\right|$ very similar to those reported in [16], as well as second-order accuracy.

For a better understanding, we have performed a specific test to investigate the effectiveness of the tail component. We used the set of exponential functions previously presented (with coefficients from Table 3.1). The time interval is retained $[0, 50\pi]$; for a fixed resolution N, the portion represented by the window is varying. The tail then fits to the part of the interval uncovered by the window. We chose different laws for $g(\tau)$ and two different resolutions. Results are shown in Fig. 3.2: the error magnitude keeps constant as N_{w} decreases while a computational saving is achieved. For the fine grid, however, we can notice an amplification of the error when the number of window points becomes too small.

3.3.2 Overall scheme

We are now able to present how the Lagrangian tracking of the dispersed phase is numerically performed. The evolution of the velocity and position of the particle is done with the third order Adams-Bashfort method:

$$\mathbf{V}^{n+1} = \mathbf{V}^n + c_{\mathrm{f1}}\left[\frac{\mathrm{d}\mathbf{V}}{\mathrm{d}t}\right]^n + c_{\mathrm{f2}}\left[\frac{\mathrm{d}\mathbf{V}}{\mathrm{d}t}\right]^{n-1} + c_{\mathrm{f3}}\left[\frac{\mathrm{d}\mathbf{V}}{\mathrm{d}t}\right]^{n-2} \tag{3.15}$$

$$\mathbf{X}^{n+1} = \mathbf{X}^n + c_{\mathrm{f1}}\,\mathbf{V}^n + c_{\mathrm{f2}}\,\mathbf{V}^{n-1} + c_{\mathrm{f3}}\,\mathbf{V}^{n-2} \tag{3.16}$$

where the square brackets with the superscript denote that each quantity is evaluated at a certain discrete time instant as for example $t_n = n\Delta t$. The characteristic coefficients of the method are assumed to be: $c_{\mathrm{f1}} = \frac{23}{12}\Delta t$, $c_{\mathrm{f2}} = -\frac{4}{3}\Delta t$ and $c_{\mathrm{f3}} = \frac{5}{12}\Delta t$ [19].

The derivative in 3.15 is evaluated from a rearranged form of the Maxey-Riley equation:

$$\left[\frac{\mathrm{d}\mathbf{V}}{\mathrm{d}t}\right]^n = k_1[\mathbf{w}]^n + k_2\left[\frac{\mathrm{d}\mathbf{u}}{\mathrm{d}t}\right]^n + k_3\frac{1}{Fr}\mathbf{e}_g + k_4[\mathbf{w}]^n \cdot \left[\nabla\mathbf{u}\right]^n + k_5[\mathbf{a}'_{\mathrm{Ba}}]^n \tag{3.17}$$

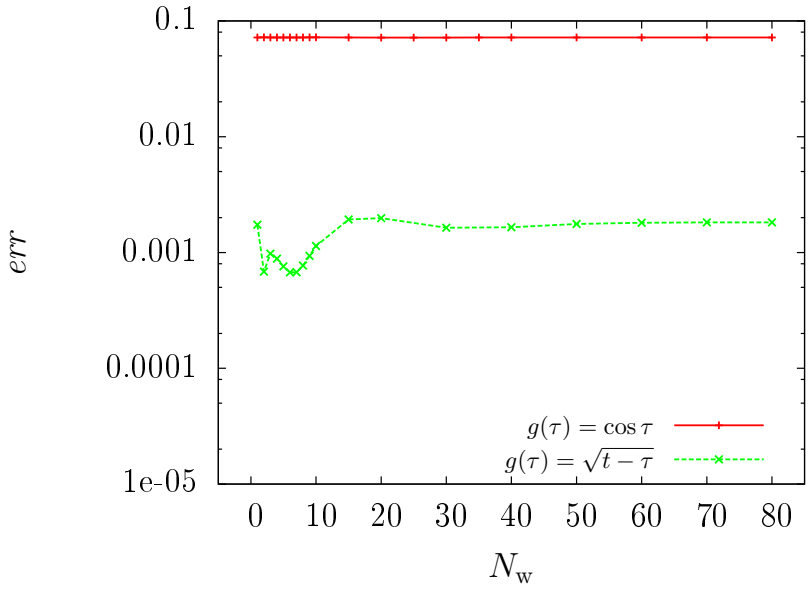

(a) $N = 81$

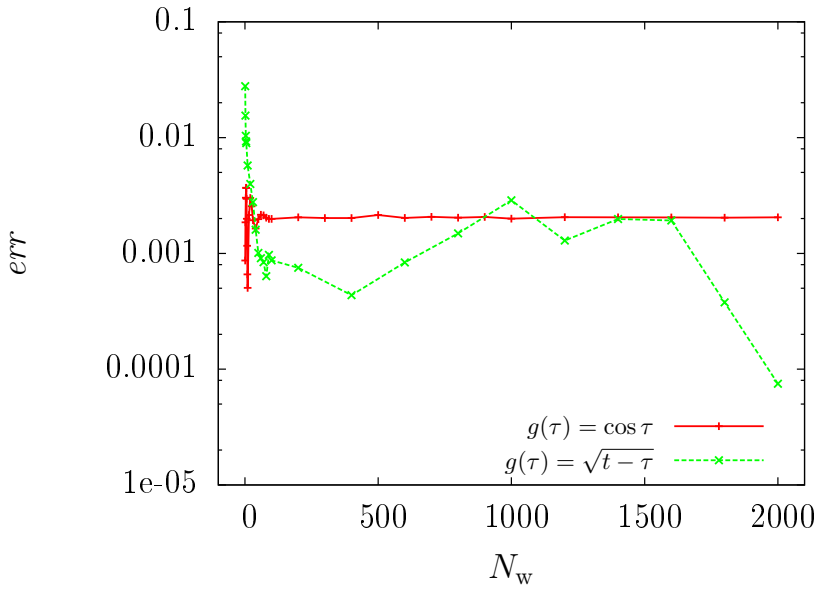

(b) $N = 2000$

Figure 3.2: *Tail effectiveness test: relative error as a function of the finite-window fraction for different $g(\tau)$, for different grid resolutions.*

where the coefficients appearing collect:

$$\begin{aligned} k_1 &= -\frac{1}{C_D \cdot St} \\ k_2 &= \frac{\frac{3}{2}\rho + \frac{4}{3}C'_{\mathrm{Ba}}\sqrt{\Delta t}}{C_D} \\ k_3 &= \frac{\rho - 1}{C_D} \\ k_4 &= -\frac{\frac{3}{2}}{C_D}\rho \\ k_5 &= -\frac{C'_{\mathrm{Ba}}}{C_D} \\ C_D &= 1 + \frac{1}{2}\rho + \frac{4}{3}C'_{\mathrm{Ba}}\sqrt{\Delta t} \end{aligned} \tag{3.18}$$

with $\rho = \rho_{\mathrm{f}}/\rho_{\mathrm{p}}$ and $C'_{\mathrm{Ba}} = C_{\mathrm{Ba}}/m_{\mathrm{p}}$; $\mathbf{a}'_{\mathrm{Ba}}$ contains all the Basset history term except the part at the present time which is collected into C_D together with the added mass part. This has to be done in order to improve numerical stability [16].

After each time-step, we need to verify that the new positions are still included in the domain. If the particle virtually crossed the border, it is basically reintroduced from the opposite side by a consistent update of the values. Finally, for certain values of the characteristic parameters, we need to evolve particles using a submultiple of the time step used for the flow to avoid numerical instability.

3.4 Validation

3.4.1 Test 1: falling particle in quiescent fluid

After the development of the code, several validation tests for the complete scheme were performed. The first one that we present concerns the classical case of a single particle falling under gravity in a fluid at rest (i.e. $u = 0$). The particle is initially at rest ($V(0) = 0$) and then approaches asymptotically its terminal velocity V_{T}. Considering the presence of the Basset History force the problem is even more challenging, also from a theoretical point of view. An analytical solution, which

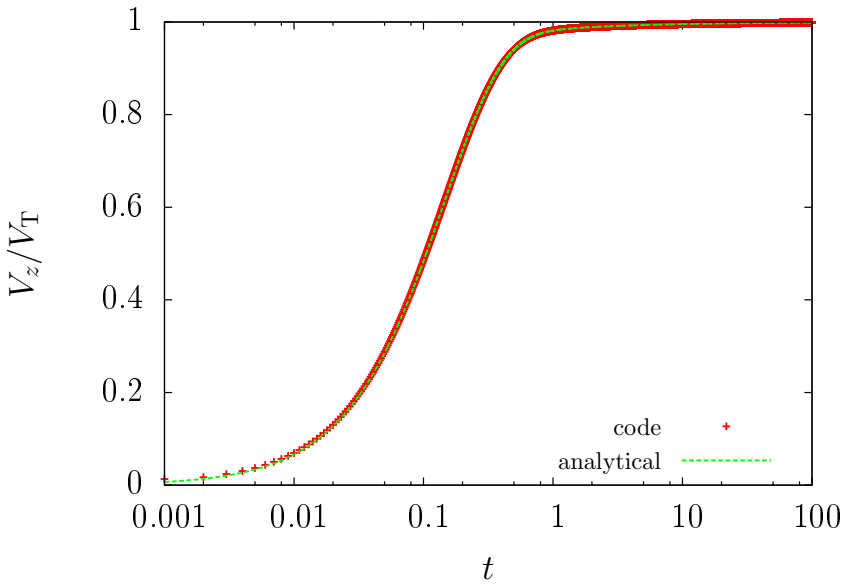

Figure 3.3: *Validation Test 1: comparison between analytical and numerical solutions in time for* $\Delta t = 0.001$

the numerical results are to be compared with, is given by Belmonte et al. in [17]:

$$V(t)/V_{\mathrm{T}}(\tau) = 1 + \frac{\sqrt{\kappa}}{\alpha - \beta}\left[\frac{e^{\alpha\tau}\,\mathrm{erfc}(\sqrt{\alpha\tau})}{\sqrt{\alpha}} - \frac{e^{\beta\tau}\,\mathrm{erfc}(\sqrt{\beta\tau})}{\sqrt{\beta}}\right] \tag{3.19}$$

where V_{T} is the terminal velocity, $\tau = t/(\tau_{\mathrm{p}}(1 + 1/2R))$, $\kappa = 9/(2R + 1)$, and $R = \rho_{\mathrm{p}}/\rho_{\mathrm{f}}$; α and β are the roots of equation $m^2 + (2 - \kappa)m + 1 = 0$. The relative error is computed on the particle velocity component in the gravity direction $V_z(t = T)$, with the final time $T = 0.1$. Results are shown in Figs. 3.3 and 3.4 for the case $St = 1$ and $R = 1000$. Fig. 3.3 presents a time history of the particle velocity, which is approaching the terminal velocity. A good agreement between numerical and analytical solution is shown. Fig. 3.4 reports the relative error for different resolutions, with a first-order accuracy that is noticed.

3.4.2 Test 2: periodic uniform fluid flow

The second test is based on the example 3 included in the Hinsberg's paper [16]. A single particle is immersed in a uniform, time-dependent periodic flow, with

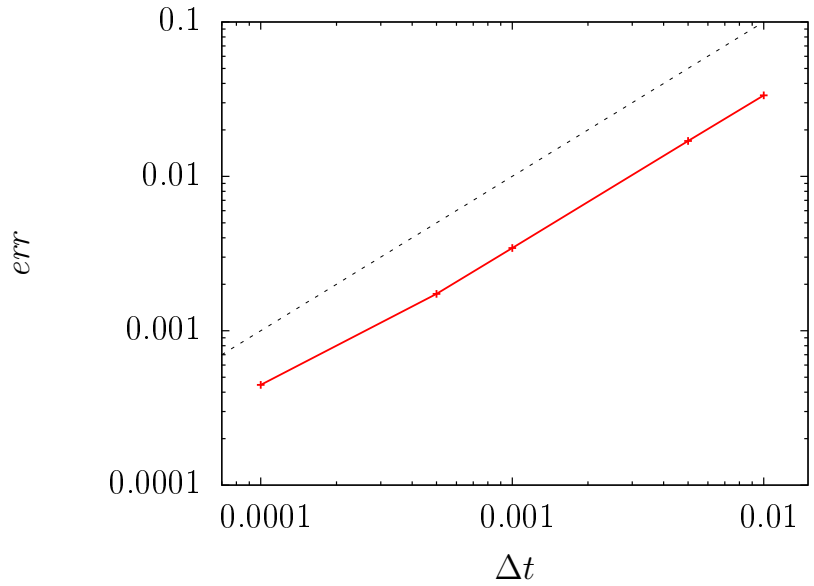

Figure 3.4: *Validation Test 1: Relative error as a function of the simulation time step. Red points are the results of the code while the black dashed line represents a first order slope.*

the following velocity field:

$$u(t) = \frac{(m_\mathrm{p} - m_\mathrm{f})g}{6\pi r_\mathrm{p}\mu}\cos 2t = \alpha \cos 2t \tag{3.20}$$

with the total force acting on particle at $t = 0$ to be null and Stokes and gravity in balance. The analytical solution is given in equation (B.7) of [16]. Fig. 3.5 shows how the numerical solution captures the analytical one.

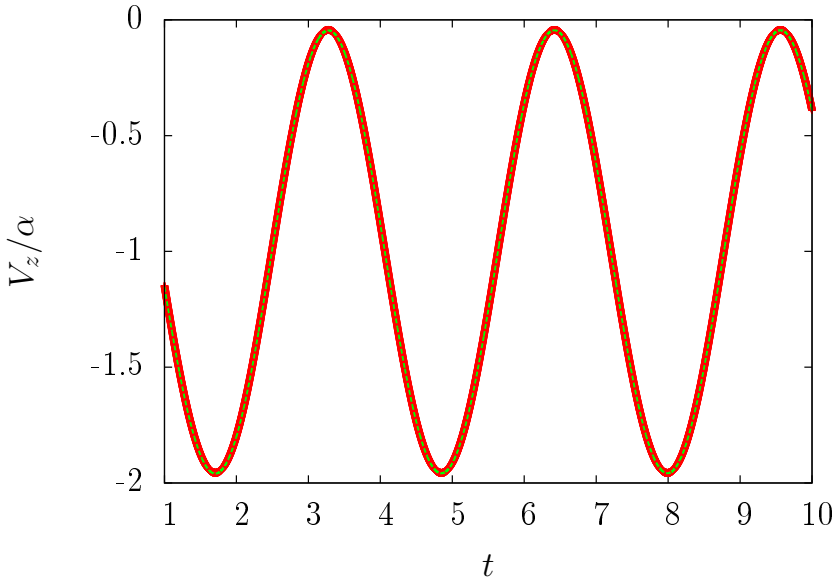

Figure 3.5: *Validation Test 2: comparison between analytical and numerical solutions in time for* $\Delta t = 0.001$ *(analytical solution: green line, numerical solution: red symbols).*

Part II

Results and Discussion

Chapter 4

General Outlook

After the description of the method given in Part I, before presenting our results, in this chapter we will report some common features for all the performed computations. These latter are basically divided in two parts:

1. a parametric investigation, exploring a wide range of the Stokes number and density ratio, in order to classify the contributions from the different forces and obtain a general review;

2. a specific focus on sedimentation of nearly neutrally-buoyant particles in turbulence.

Simulations were performed at KTH Mechanics[1] and *Matrix* supercomputer at CASPUR[2], using an OpenMP parallelization. Before illustrating in detail each part, the common features are described.

4.1 Flow solver features

All simulations were performed using 288^3 wavenumbers on a cubic domain of side $\mathcal{L} = 2\pi$. The turbulence is characterized only by the Taylor Reynolds number $Re_\lambda = u'\lambda/\nu \simeq 136$, based on the Taylor lengthscale $\lambda = \sqrt{\epsilon/(15\nu u'^2)}$ and the root-mean-square of the fluid velocity fluctuations u'.

[1] `http://www.mech.kth.se`
[2] `http://www.caspur.it/infrastrutture/cluster-hpc-matrix`

4.2 Particle tracking features

Fixing the flow conditions, i.e. the Reynolds number, the particle dynamics depends only on three dimensionless parameters: the density ratio $R = \rho_\mathrm{p}/\rho_\mathrm{f}$, the Stokes number $St_\mathrm{K} = \tau_\mathrm{p}/\tau_\mathrm{K}$, and the Froude number $Fr = U/(g\tau_\mathrm{ref})$.

For all simulations:

- fully developed turbulent regime is first obtained without the presence of particles;
- N_p particles are then released into the domain with an uniform random distribution;
- particles are initially set at the same velocity of the flow (zero relative velocity), plus the terminal falling velocity in the gravity direction:

$$\mathbf{V}(0) = \mathbf{u}(\mathbf{X}(0), 0) + \mathbf{V}_\mathrm{T} \tag{4.1}$$

  with $\mathbf{V}_\mathrm{T} = V_\mathrm{T}\,\mathbf{e}_g$
- their evolution is then computed over a time T, saving snapshots of particles quantities at each 0.1 time units in order to compute statistics.

4.3 Statistical postprocessing

Results of simulations are then elaborated and some specific statistical quantities are obtained, which we define for completeness in the following.

4.3.1 P.d.f.'s of the acceleration ratios

An important quantity in the analysis of turbulent flows is the p.d.f. (*probability density function*), that gives a clear indication on many statistical properties, not only the mean value but also higher-order characteristics. We focus on the p.d.f. of the accelerations, that are stricly related to the forces.

Since we are in homogeneous and isotropic turbulence, the expected values of the acting forces and accelerations (including the total one) are null. Therefore

we will examine the p.d.f. of the different acceleration sources, considering the p.d.f. of each term on the r.h.s. of the Maxey-Riley equation divided by the total particle acceleration (i.e. the l.h.s.),

$$1 = \frac{a_{\mathrm{SD}}}{a_{\mathrm{p}}} + \frac{a_{\mathrm{PG}}}{a_{\mathrm{p}}} + \frac{a_{\mathrm{Gr}}}{a_{\mathrm{p}}} + \frac{a_{\mathrm{AM}}}{a_{\mathrm{p}}} + \frac{a_{\mathrm{Ba}}}{a_{\mathrm{p}}} \tag{4.2}$$

where $a_{\mathrm{p}} = \frac{\mathrm{d}V}{\mathrm{d}t}$ and the other terms denote vector components and not the modulus. By computing the p.d.f. of each of the quantities appearing above, a clear indication of the dominant force will be obtained. Expected values around 1 will indicate a component that basically determines alone the overall instantaneous particle acceleration.

4.3.2 Radial distribution function

The *radial distribution function*, usually denoted $g(r)$, measures the probability of finding a particle pair at a distance r normalized with that of a purely random Poissonian arrangement and is calculated in order to investigate the particle distribution in space and the clustering intensity.

In other words, it can be expressed as the ratio between the actual number of particles inside an infinitesimally thin shell of radius r centred on a given particle and the number that would be expected if the particles were uniformly distributed. Hence, the radial distribution function indicates the existence of accumulation effects (i.e. particles creating clusters in specific regions).

Chapter 5

Parametric Investigation

Several forces act on particles dispersed in turbulent flows. The relative importance of each force strongly depends on the values of the characteristic parameters: the density ratio $R = \rho_p/\rho_f$ and the Stokes number St_K. The first aim of our work is to review the widest possible range of these values, focusing on the relative particle dynamics.

5.1 Simulation features

A parametric survey was therefore performed considering 10 different combinations of $R = \rho_p/\rho_f$ and St_K. Tables 5.1 and 5.2 show the set of considered values. $R = 1$ and $R = 10$ well reproduce the behaviour of small solid particles in liquids, while

Table 5.1: *Crosstab reporting the investigated cases. The bold number represents the case number. The row and column position indicate respectively its density ratio and Stokes number.*

R \ St_K	0.01	0.1	1	10
0.1	**1**			
1	**2**	**5**		
10	**3**	**6**	**8**	
1000	**4**	**7**	**9**	**10**

Table 5.2: *List of the investigated cases. The bold number represents the case number.*

Case	R	St_{K}
1	0.1	0.01
2	1	0.01
3	10	0.01
4	1000	0.01
5	1	0.1
6	10	0.1
7	1000	0.1
8	10	1
9	1000	1
10	1000	10

$R = 1000$ is typical of aerosol/droplets in gases. The Stokes numbers are selected to avoid particles larger than the hydrodynamic lengths, so within the limits of our model. The gravitational force is here neglected in order to decrease the number of indipendent variables, i.e. $Fr = \infty$. For each case, $N_{\mathrm{p}} = 100000$ particles are considered. For each parameter set, we performed simulations with and without the Basset History force for comparison. We have simulated the unladen fluid phase until reaching the fully developed turbulent regime, when the particles are introduced with a random spatial distribution and the velocity of the fluid at the same position. We evolve the particle-fluid system for a time $T \simeq 700\tau_{\mathrm{K}}$ and save snapshots of particles quantities every $0.7\tau_{\mathrm{K}}$ time units in order to compute statistics.

5.2 Results

5.2.1 Force contributions

The p.d.f.'s of the ratios between each acceleration and the total[1], representative of the force contributions, are reported systematically, case by case, in Appendix C,

[1]The choice of this quantity to be investigated has been discussed in §4.3.1

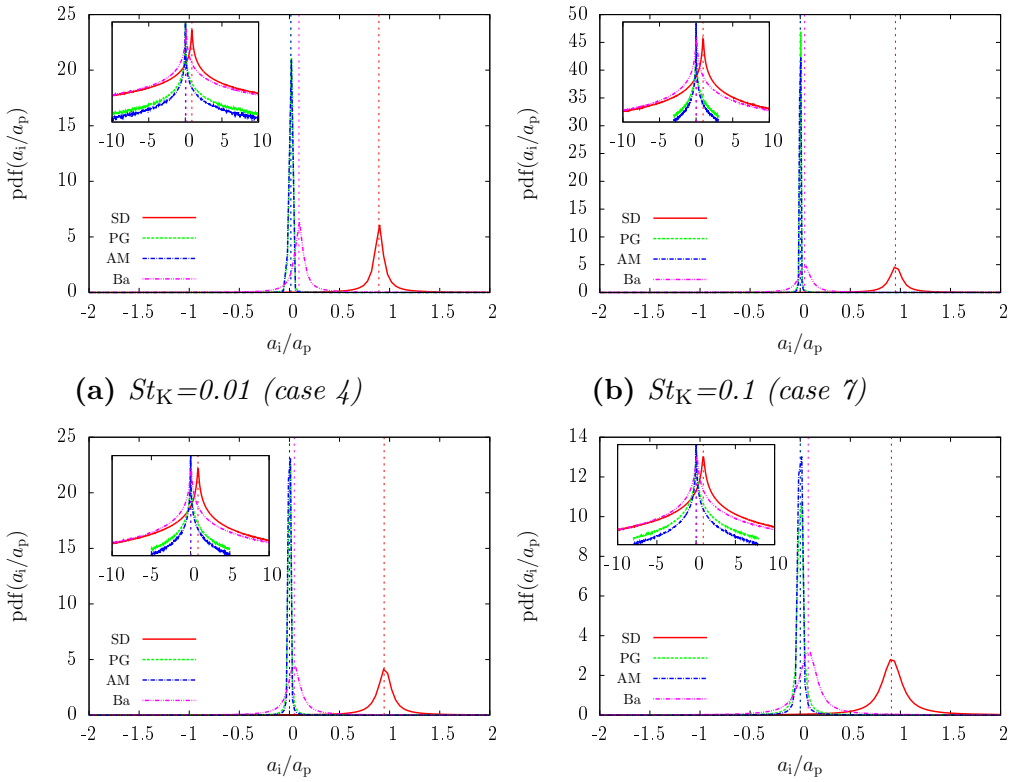

(a) *St_K=0.01 (case 4)* **(b)** *St_K=0.1 (case 7)*

(c) *St_K=1 (case 9)* **(d)** *St_K=10 (case 10)*

Figure 5.1: *P.d.f.'s of the different acceleration ratios a_i/a_p for particles with $R = 1000$ (heavy particles).*

while here we recollect those with the same density ratio R together. From the figures we deduce the following points:

- for the highest density ratio $R = 1000$ (proper of particles usually denoted as *heavy*), the dominant term is found to be the Stokes Drag, in agreement with the often recurring practice [38]. However, we notice that the Basset force has always a certain, although relatively small, relevance. A related overall picture is given in Fig. 5.1;

- the case of *neutrally-buoyant* particles ($R = 1$) presents a totally different behaviour (Fig. 5.2), with the Pressure Gradient as the leading term; particles tend to approximate the behaviour of fluid elements, even if the Stokes Drag interestingly increases when the Stokes number becomes smaller;

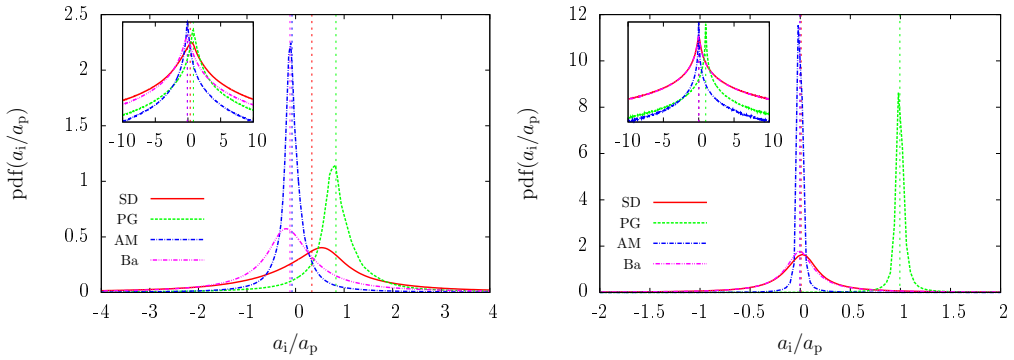

(a) *St_K=0.01 (case 2)* **(b)** *St_K=0.1 (case 5)*

Figure 5.2: *P.d.f.'s of the different acceleration ratios a_i/a_p for particles with $R = 1$ (neutrally-buoyant particles).*

- for intermediate density ratios ($R = 10$) we do not have one dominant force, while we find a cross-over between the different, as shown in Fig. 5.3;
- for lighter-than-fluid particles (case 1) the mean value of the Pressure Gradient term is several times the particle acceleration while other forces counteract (mainly Basset and Added Mass);
- the Basset History force has a small but non-zero mean value for almost all cases;
- the Added Mass term is the smallest in nearly all cases except for lighter-than-fluid particles.

Some of these trends are not surprising if we look at the Maxey-Riley equation, as we discussed its limits (§2.2.3). In this regard, the numerical results confirm the validity of some often done approximations, especially for heavy particles. Taking into account all the forces, however, we find some insights for a more general view, such as for example the existence of a small contribution from the Basset force, still referring to high density ratio cases. We will deepen this latter point in the next section.

The semi-log views (reported in the insets of the previously cited figures) indicate the type of probability distribution we are dealing with: a non-gaussian behaviour is always found for all cases. The dispersion is wider with respect to

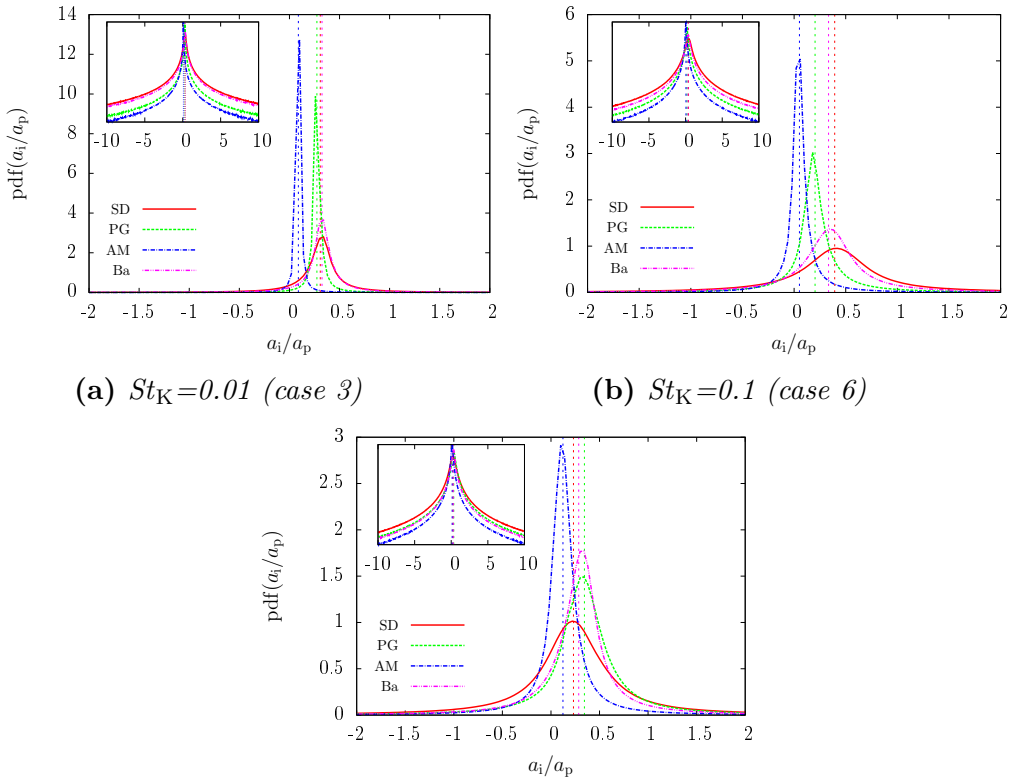

(a) *St_K=0.01 (case 3)* **(b)** *St_K=0.1 (case 6)*

(c) *St_K=1 (case 8)*

Figure 5.3: *P.d.f.'s of the different acceleration ratios a_i/a_p for particles with $R = 10$ (intermediate density ratio).*

the equivalent gaussian distribution, with the same mean value and standard deviation. An explanatory example is built up in Fig. 5.4. We notice in particular that the viscous forces (Stokes Drag and Basset) constantly exhibit the largest tails.

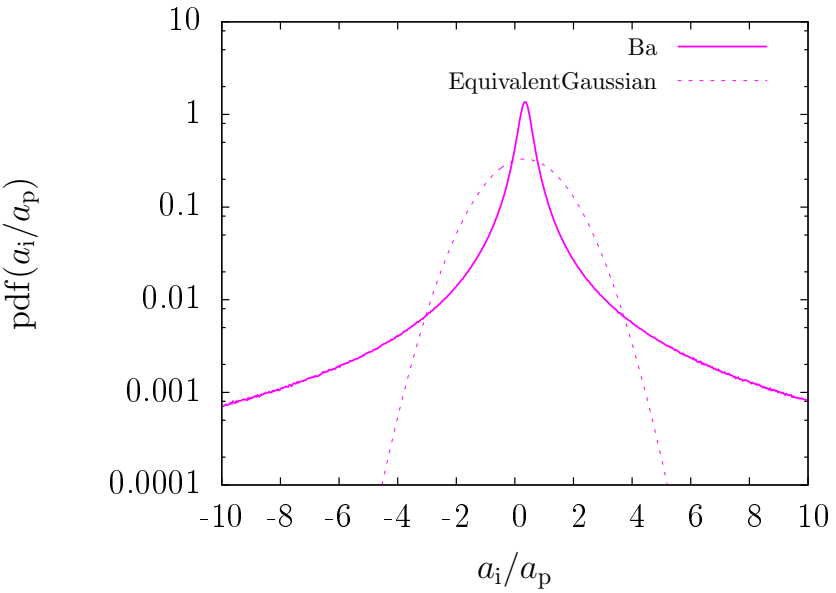

Figure 5.4: *Comparison between the obtained p.d.f. and the equivalent gaussian distribution with the same mean value and standard deviation, for the Basset curve of case 6 ($R = 10$, $St_K = 0.1$).*

5.2.2 Role of the Basset History force

As we stated several times so far, the Basset History force represents a challenging term both from a theoretical and computational point of view and is often neglected. For this reason it could be interesting to compare the results between computations that take into account or neglect the Basset History force. The same cases were therefore simulated again deactivating the computation of the Basset term and the results compared with the Basset-activated simulations.

Fig. 5.5 shows a comparison for two of the heavy particles cases. In the simulations without the Basset force, the Stokes Drag present a narrow distribution

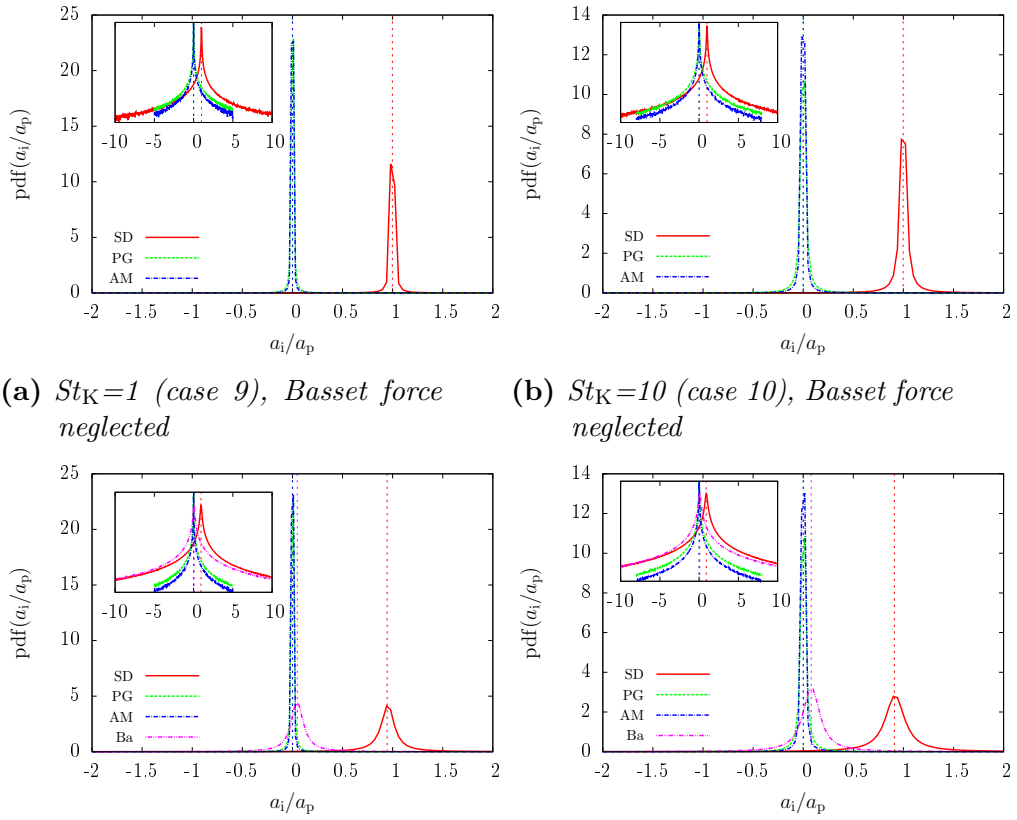

(a) *St_K=1 (case 9), Basset force neglected*

(b) *St_K=10 (case 10), Basset force neglected*

(c) *St_K=1 (case 9), Basset force included*

(d) *St_K=10 (case 10), Basset force included*

Figure 5.5: *P.d.f.'s of the different acceleration ratios a_i/a_p for particles with $R = 1000$ (heavy particles). Comparison between simulations with and without the Basset History term computation.*

whose average lies around 1, while the distribution of the Pressure Gradient and the Added Mass both could be approximated by Dirac-delta functions centered on 0. In other words, the Stokes Drag is the leading term driving the particle acceleration, in agreement with the usual assumptions in literature. The Basset force, however, does have an impact on the inertial particle dynamics as displayed in the bottom panels. Its presence widens the p.d.f. of the Stokes Drag, and more importantly, moves its average to a value of about 0.9 (vertical dashed lines in the figure). Even at this high density ratio, the Basset force influences the overall particle acceleration in an appreciable way. In addition, the lin-log plots in the insets reveal that both the SD and the BH exhibit long tails; rare intense events are even more influenced by the Basset History term. Particles with different Stokes number show a similar behavior (not reported here).

For particles of density ratio $R = 1$, we see in Fig. 5.6 that, for the case with smallest Stokes number, the leading term in the balance is the Stokes Drag when Basset is not considered, whereas it becomes the Pressure Gradient with the full model. Even for this case, we note the very long tails in the distribution of the Stokes Drag.

Finally, the behavior of particles with an intermediate density ratio, $R = 10$, is presented in Fig. 5.7. Unlike the case of particles with $R = 1000$, we do not find one dominant term, but the particle dynamics emerge from the contribution of the different forces, with significantly long tails. Examining the simulations where BH is not considered, figs. (a) and (b), we note that the PG becomes more and more important with respect to the SD when increasing the Stokes number. Most importantly, the impact of the BH is relevant for all Stokes numbers considered (see figs. (c) and (d)). Indeed, the average impact of the other terms, SD in particular, is strongly altered by the presence of the BH. Hence, at density ratios of the order $R \approx 10$, BH cannot be neglected to capture the correct particle dynamics.

5.2.3 Particles distribution

As stated in the introduction, a point of interest in the study of particle-laden flows concerns the particle distribution in space, since some peculiar behaviours

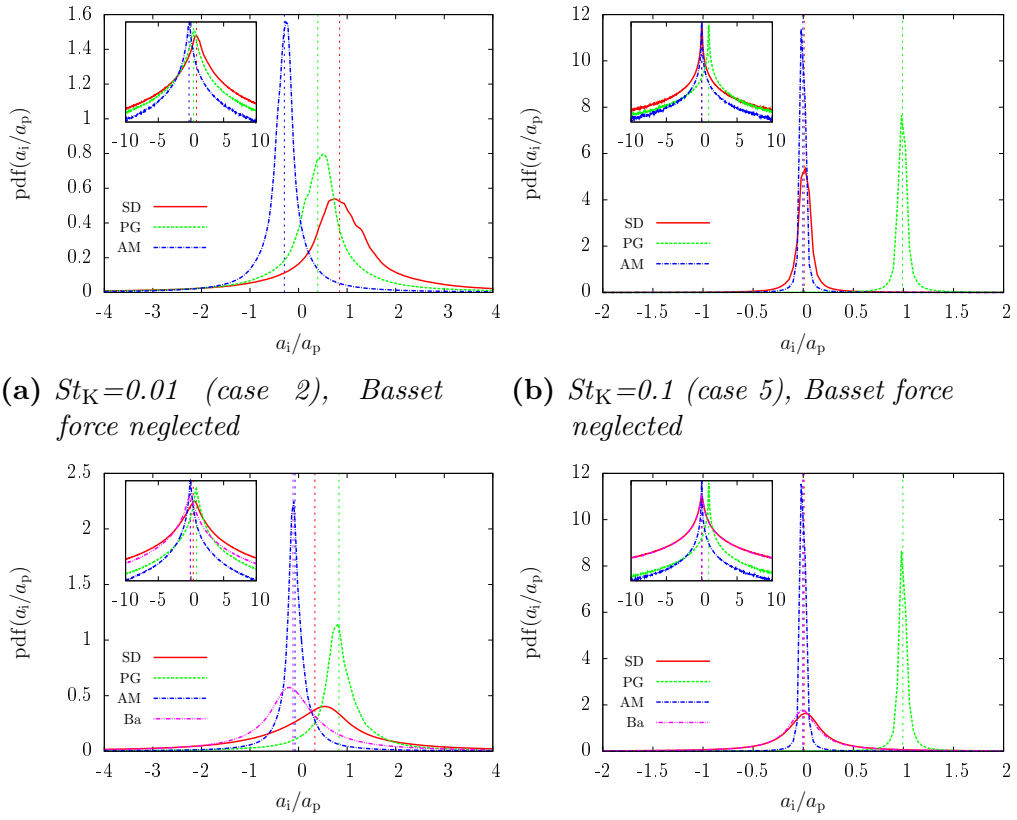

(a) *St_K=0.01 (case 2), Basset force neglected*

(b) *St_K=0.1 (case 5), Basset force neglected*

(c) *St_K=0.01 (case 2), Basset force included*

(d) *St_K=0.1 (case 5), Basset force included*

Figure 5.6: *P.d.f.'s of the different acceleration ratios a_i/a_p for particles with $R = 1$ (neutrally-buoyant particles). Comparison between simulations with and without the Basset History term computation.*

are found, such as the possible formation of clusters, also denoted in literature as *preferential accumulation* [38].

Some illustrative screenshots of the particle position are given in Figs. 5.8 to 5.10, depicting a slice of finite thickness from the domain (parallel to the xy plane and taken at the middle of the z-axis[2]) and showing the particle distribution at a certain time. Results in fig. (a) are obtained without the Basset History term as it was often assumed in previous numerical studies on particle-laden turbulent

[2]We recall however that the system is isotropic and gravity is neglected, hence the choice of the plane is arbitrary.

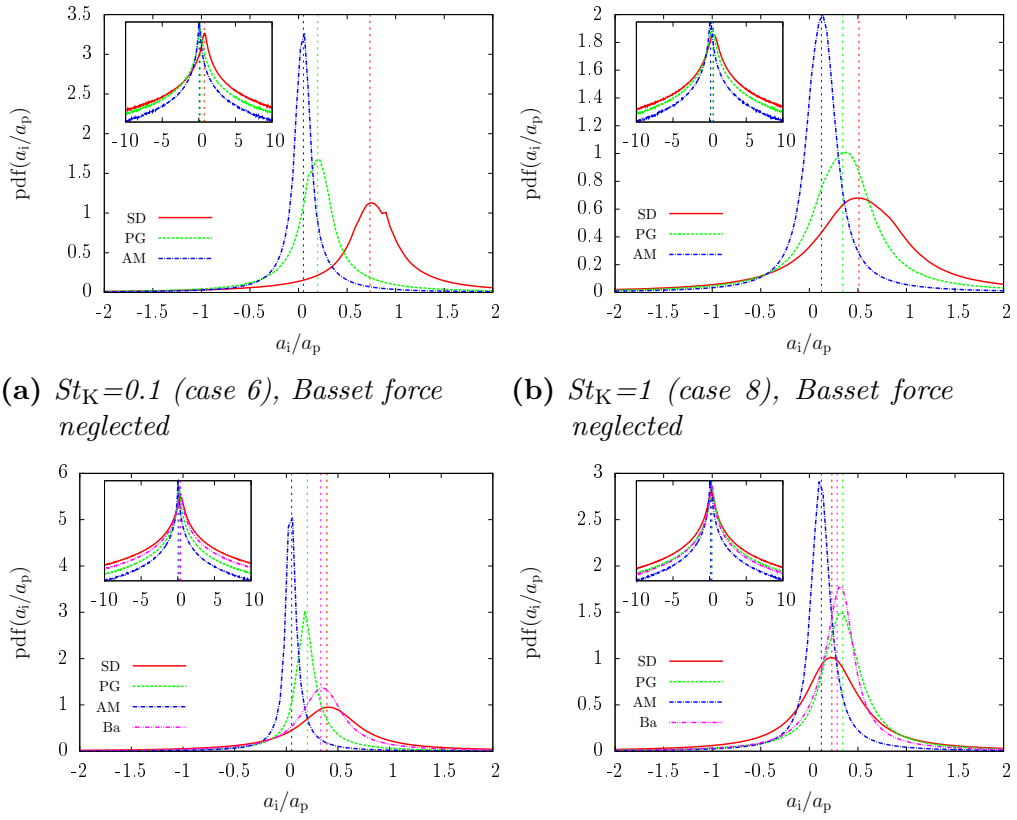

(a) *St_K=0.1 (case 6), Basset force neglected*

(b) *St_K=1 (case 8), Basset force neglected*

(c) *St_K=0.1 (case 6), Basset force included*

(d) *St_K=1 (case 8), Basset force included*

Figure 5.7: *P.d.f.'s of the different acceleration ratios a_i/a_p for particles with $R = 10$ (intermediate density ratio). Comparison between simulations with and without the Basset History term computation.*

flows, while fig. (b) is relative to simulations with the complete evaluation of all the forces. Small-scale clustering characterizes the particle distribution: clusters and void regions large enough to be clearly appreciated at first sight. When the BH term is included, the particle segregation appears to be less intense, i.e. the Basset History term acts to smear out the clusters, as it was also recently observed in chaotic bi-dimensional flows [12]. Interestingly this effect appears also for particles at high density ratios, i.e. $R = 1000$.

In this regard, the radial distribution function is a useful tool for measuring the clustering intensity; calculated values for all cases are reported in Fig. 5.11,

both for simulations with and without the Basset force taken into account. The highest accumulation is found for heavy particles with response time of the same order of the small-scales (case 9), in agreement with literature indications [39]. Lighter-than-fluid particles (case 1) show significant clusters, especially if the Basset term is neglected. Cases with the lowest Stokes number and $R = 1 \div 1000$ (cases from 2 to 4) and neutrally-buoyant particles (case 2 and 5), on the other hand, always exhibit a flat $g(r)$ which means a nearly uniform, tracer-like, local distribution. For every density ratio, we find the highest levels of small-scale clustering when $St_{\mathrm{K}} = 1$, while the accumulation is weaker for the other Stokes numbers considered, in agreement with previous findings [38]. The major insight is that the Stokes number acts as the primary governing parameter.

In a similar way as we did before, we focus on the effect of the Basset History term. The RDF for some of the most representative cases is reported in 5.12 where we compare the data obtained with (lines) and without (symbols) considering the Basset force. For all cases, the effect of the Basset term is to weaken the clustering, confirming the visual impression given in the screenshots presented before. Particles with $R = 1$ or tiny St_{K} do not show clustering, and this does

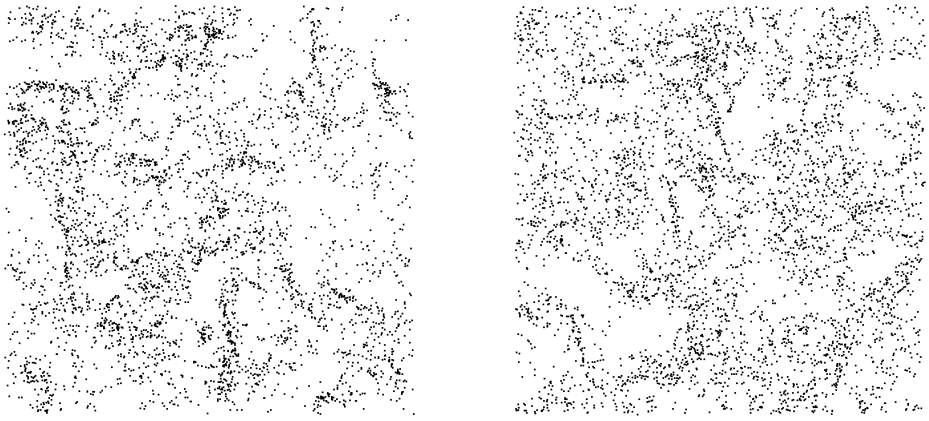

(a) *without Basset term* **(b)** *with Basset term*

Figure 5.8: *Screenshots of particles distribution at $R = 10$, $St_K = 1$ (case 8). Comparison between simulations with and without the Basset History term computation.*

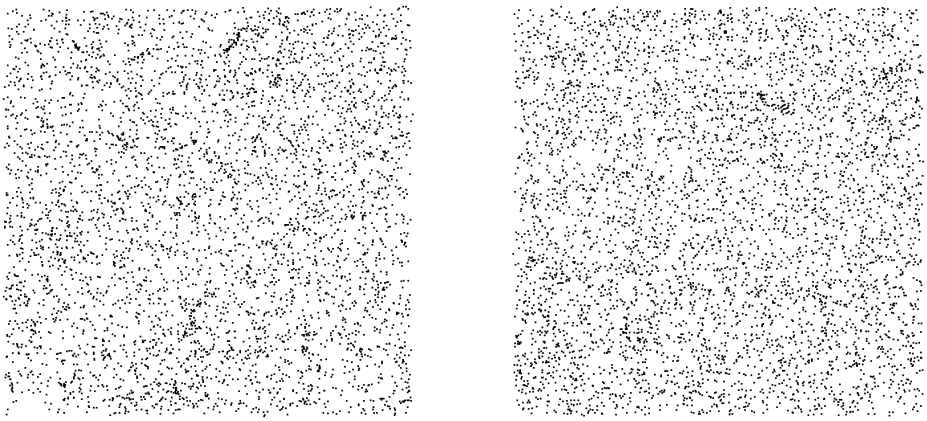

(a) *without Basset term* **(b)** *with Basset term*

Figure 5.9: *Screenshots of particles distribution at* $R = 0.1$, $St_K = 0.01$ *(case 1). Comparison between simulations with and without the Basset History term computation.*

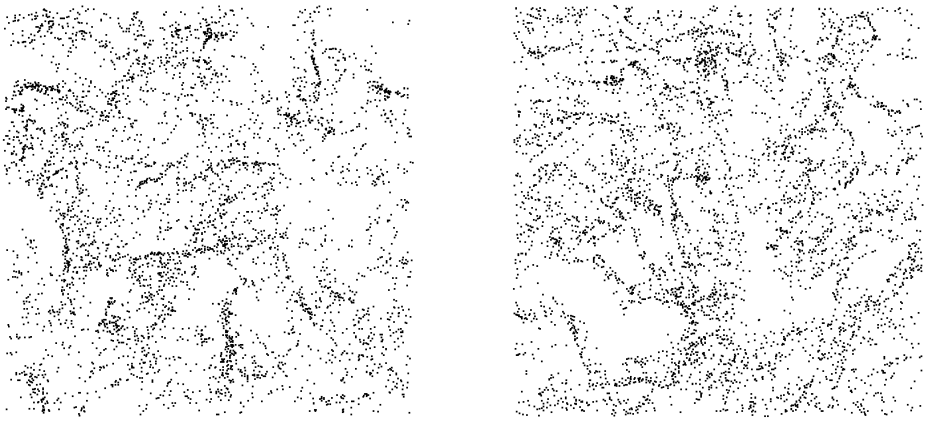

(a) *without Basset term* **(b)** *with Basset term*

Figure 5.10: *Screenshots of particles distribution at* $R = 1000$, $St_K = 1$ *(case 9). Comparison between simulations with and without the Basset History term computation.*

not change including the Basset term.

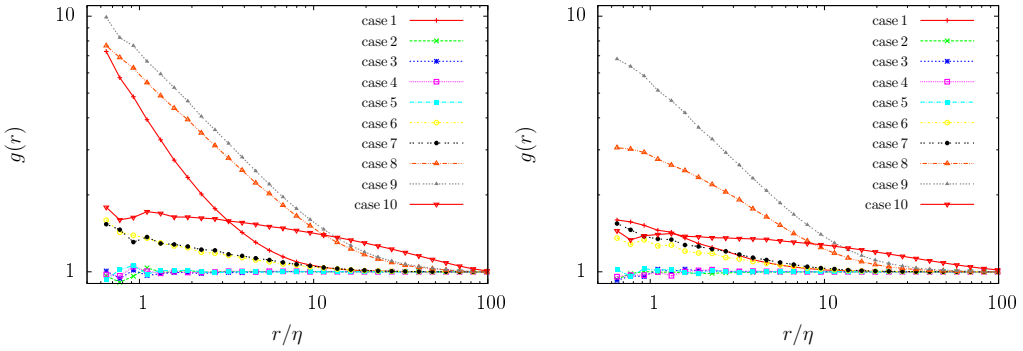

(a) *without Basset term* **(b)** *with Basset term*

Figure 5.11: *The radial distribution function $g(r)$ versus particle distance r/η. Comparison between simulations with and without the Basset History term computation.*

5.3 Remarks

The results of the present chapter aim to give a clear indication of the very different dynamics that particles can experience depending on the density ratio and Stokes number. Furthermore a special focus is made on the role of the Basset History force, by comparing results between simulations that neglect or not its presence.

Different Stokes numbers and density ratios have been considered. For heavy particles ($R = 1000$) the Stokes Drag is the dominant term with a small contribution of the Basset force, while for neutrally-buoyant particles ($R = 1$) the Pressure Gradient becomes the prevailing term. For intermediate density ratios no dominant force is found and a complete evaluation of all terms will be appropriate. The clustering intensity is found to depend mainly on the Stokes number, with a maximum intensity around $St_{\mathrm{K}} = 1$, in agreement with many results in literature.

The BH is found to be relevant in the dynamics of particles with moderate density ratios, $R = 1$ and $R = 10$, where its presence alters the balance of the different terms that determine the particle acceleration. This has a relevant impact on the small-scale clustering observed at $R = 10$. The result on the impact of BH on the dynamics of particles with high density ratio, $R = 1000$ is even more unexpected. Also here, the clustering intensity is found to decrease for

Stokes number in the range $St_K = 10.1 \div 10$. Examining the p.d.f.'s of the terms determining the total particle acceleration, BH amount to $\sim 10\%$ of the total. For the rest, the particle acceleration is determined by the Stokes Drag. It is also worth noting that the p.d.f.'s of the BH show long tails, meaning that this force is crucial for a correct representation of rare intense events on the particle dynamics.

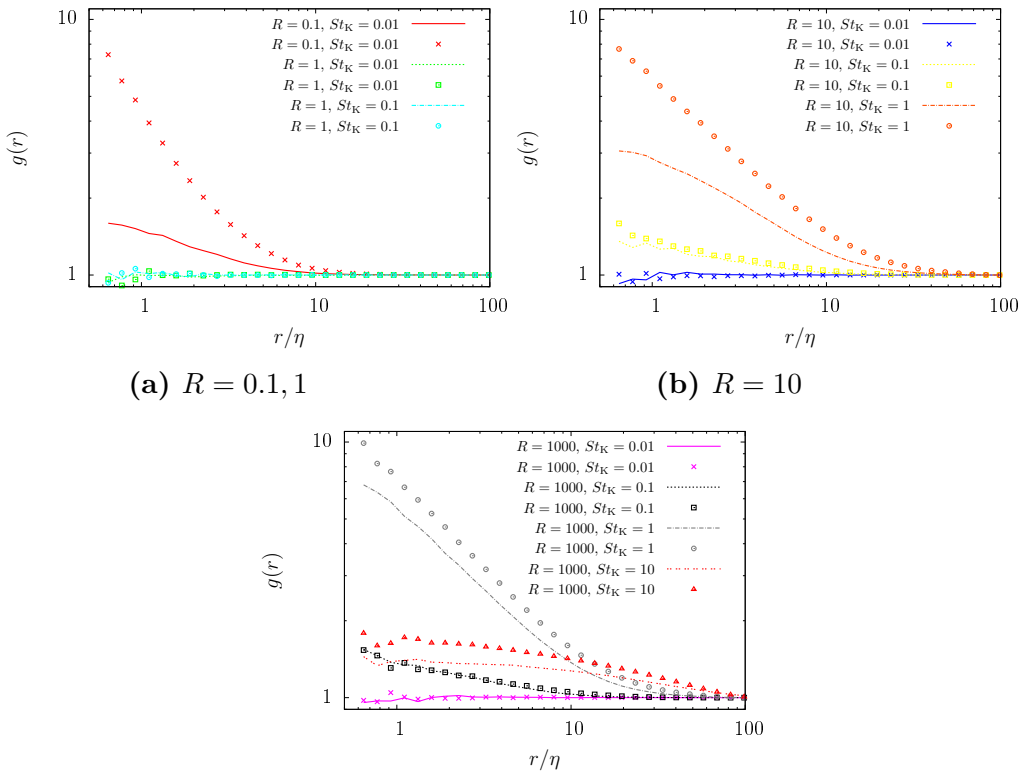

(a) $R = 0.1, 1$ **(b)** $R = 10$

(c) $R = 1000$

Figure 5.12: *The radial distribution function $g(r)$ versus particle distance r/η for different R. Results including the Basset term are displayed by solid lines, results without Basset with symbols*

Chapter 6

Sedimentation of nearly neutrally-buoyant particles

6.1 Introduction

One interesting topic within the framework of particle-laden flows is the effect of turbulence on the mean settling rate of particles. Basically the question is: "Does turbulence enhance the settling (or floating) of particles?". It is a well-known fact that a spherical object immersed in a quiescent fluid, in the presence of gravity, will asymptotically reach a so-called terminal velocity. What happens if the fluid is moving and, in particular, in the case of a turbulent flow? The answer is not trivial and it has been investigated by several works [14, 40]. If we refer to homogeneous, isotropic turbulence, it is not easy to make a prediction of this effect in an intuitive way, since the mean values of the fluid velocity and acceleration are null. Wang and Maxey [39] showed that in the case of heavy particles ($\rho_\mathrm{p}/\rho_\mathrm{f} > 100$) turbulence induces a relevant increase of the mean settling velocity.

A field in which this problem becomes particularly relevant is the study of microorganisms dispersed in water such as *phytoplankton* in the ocean. In marine biology, the understanding of the role of turbulence on these species, and in particular on their sinking or floating properties, is a debated topic with relevant connections to ecological processes [32, 34, 28]. We decided to focus on this

specific range. As a first approximation, we treat plankton like particles, even if a more detailed approach should consider a proper shape description and possible swimming properties. Nevertheless, we can give a useful contribution to the investigation of this interesting problem by using the tools we have developed so far.

On this purpose will be to calculate the average settling velocity of particles and we will compare this result to the terminal velocity of the falling particle in a fluid at rest, in order to see if a significant difference exists.

6.1.1 Terminal velocity

We briefly recall the reference situation with which the effect of turbulence, if any, will be assessed. We consider a single particle immersed in still fluid, hence $\mathbf{u}(\mathbf{x}, t) = \mathbf{0}$. It is well-known that the viscous drag will gradually increase with the particle velocity. For $t \to \infty$ this force will balance the gravitational and buoyancy effect so that the falling particle will asymptotically tend to a finite limit, the so-called *terminal velocity* $\mathbf{V}_\mathrm{T}$ [8]. This limit can be found by setting to zero all the unsteady terms in the Maxey-Riley equation, hence:

$$\mathbf{V}_\mathrm{T} = \tau_\mathrm{p}(1 - \frac{\rho_\mathrm{f}}{\rho_\mathrm{p}})\mathbf{g} \tag{6.1}$$

which is the classical result from G. G. Stokes. Here, τ_p is the particle relaxation time, ρ_p and ρ_f are the particle and fluid densities, respectively, and $\mathbf{g}$ is the gravity vector.

6.1.2 Range of parameters

We need to estimate the representative values for phytoplankton in the ocean. We note that for these microorganisms a detailed measurement of certain properties such as the geometric dimensions is very difficult [32]. However, we can delineate an adequate set of parameters to be as follows:

- the density ratio varies within $\rho_\mathrm{p}/\rho_\mathrm{f} = 1.01 \div 1.05$;

- values of the turbulent mean dissipation rate for the ocean can be assumed to vary within $\epsilon = 10^{-7} \div 10^{-4}\,\mathrm{m}^2/s^3$;
- the equivalent Stokes diameter, i.e. the particle diameter, is assumed to vary within $d = 1 \div 100\mu\mathrm{m}$;
- the kinematic viscosity of water is assumed to be $\nu = 10^{-6}\mathrm{m}^2/s$.

6.2 Simulation features

In order to investigate the problem, we performed Direct Numerical Simulations with the same basic features presented in Chapter 4. The following set of nondimensional parameters was chosen for our computations:

Case	$\frac{\rho_\mathrm{p}}{\rho_\mathrm{f}}$	St_K	$\frac{V_\mathrm{T}}{u_\mathrm{K}}$
A	1.05	0.01561	0.0133
B	1.01	0.00096	0.0419

which can be equivalent to the following dimensional values:

Case	$\frac{\rho_\mathrm{p}}{\rho_\mathrm{f}}$	$\epsilon_\mathrm{T}\,[\mathrm{m}^2/\mathrm{s}^3]$	$d\,[\mu\mathrm{m}]$
A	1.05	10^{-4}	166
B	1.01	$3 \cdot 10^{-6}$	100

with $\nu = 10^{-6}\mathrm{m}^2/\mathrm{s}$ and $g = 9.81\mathrm{m}/\mathrm{s}^2$.

In this case, the procedure is characterized by these particular features:

- 3 populations ($N_\mathrm{p} = 200000$ particles each) are considered in order to speed up the statistical convergence, with gravity respectively directed towards $-x$, $-y$ and $-z$;
- the settling velocity, which is the result of main interest, is calculated as

follows:

$$\langle V_{\mathrm{S}}\rangle(t) = \frac{1}{N_{\mathrm{p}}}\left[\sum_{p=1}^{\frac{N_{\mathrm{p}}}{3}} V_x(t) + \sum_{p=\frac{N_{\mathrm{p}}}{3}+1}^{\frac{2}{3}N_{\mathrm{p}}} V_y(t) + \sum_{p=\frac{2}{3}N_{\mathrm{p}}+1}^{N_{\mathrm{p}}} V_z(t)\right] \tag{6.2}$$

where the three summations reflect the different populations mentioned above and p is a counter for particle. Eq. (6.2) provides an average over the total number of particles and over the different populations. Furthermore a third average is performed in time:

$$\overline{\langle V_{\mathrm{S}}\rangle} = \frac{1}{T_{\mathrm{f}} - T_{\mathrm{i}}}\int_{T_{\mathrm{i}}}^{T_{\mathrm{f}}} \langle V_{\mathrm{S}}\rangle(t)\,\mathrm{d}t \tag{6.3}$$

with T_{i} and T_{f} are the initial and final time of evaluation.

- the simulation time reached $T \simeq 1540\tau_{\mathrm{K}}$.

6.3 Results

6.3.1 Settling velocity

Figs. 6.1 and 6.2 report the time history of the average settling velocity $\langle V_{\mathrm{S}}\rangle$, together with the further average over time $\overline{\langle V_{\mathrm{S}}\rangle}$ (blue dashed line), showing its progressive convergence. The relative variation of the mean settling velocity $(\overline{\langle V_{\mathrm{S}}\rangle} - V_{\mathrm{T}})/|V_{\mathrm{T}}|$ evaluated at the final time T[1] is found to be about -14% for case A (the minus means that turbulence increases the sedimentation rate) while for case B we found a value about $+2\%$ i.e. sedimentation is slightly weakened. We could affirm that no dramatic variation of settling velocity is noted.

As a further deepening, we can derive the following relation from the Maxey-Riley equation:

$$\overline{\langle V_{\mathrm{S}}\rangle} - V_{\mathrm{T}} = \overline{\langle u\rangle}\Big|_{\mathrm{p}} - \tau_{\mathrm{p}}\left(\langle a_{\mathrm{PG}}\rangle + \langle a_{\mathrm{Ba}}\rangle + \langle a_{\mathrm{AM}}\rangle\right)\Big|_{\mathrm{p}} \tag{6.4}$$

[1] computed from $t = 280\tau_{\mathrm{K}}$ in order to avoid the initial transient.

where the various quantities are sampled at the particle position and averaged over particles and time. We find that the first term at the right-hand-side is much larger than the second term related with the three accelerations. Hence, the tiny increase of settling velocity has to be related with a certain preferential sampling of the flow and not to a direct effect from any of the forces. On the other hand, the overall picture could suggest the relevance of a statistical error.

These results could be compared with recent experimental results [34], with surprising differences. However, what we found seems to be in agreement with expectations based on the present values of the Stokes number and density ratio. As we discussed in the previous chapter, this range is typically characterized by low clustering effects and a tracer-like behaviour.

Finally, it is important to note that the results by Wang and Maxey [39], cited in the introduction of this chapter, are relative to values of St_{K} and $\rho_{\mathrm{p}}/\rho_{\mathrm{f}}$ substantially different from those we have chosen for this investigation. The overall situation is thus: the mean settling rate is strongly modified when St_{K}

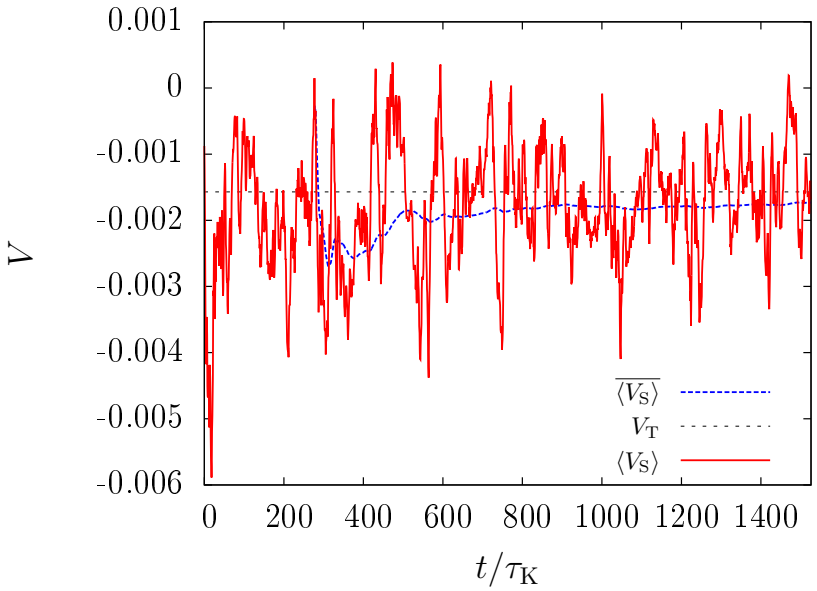

Figure 6.1: *Settling velocity, case A. The red curve is the settling velocity averaged over the particles, the blue dashed line its time average, while the black dashed line indicates the theoretical terminal velocity.*

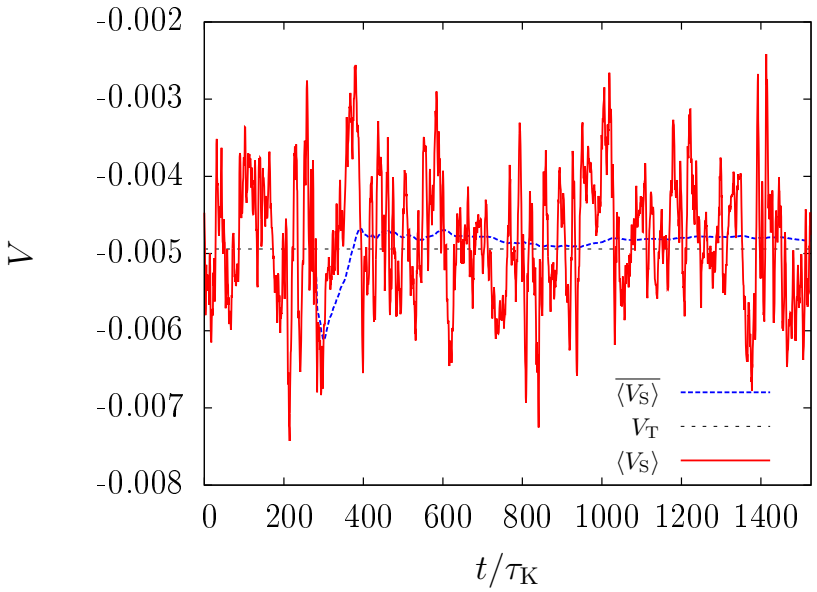

Figure 6.2: *Settling velocity, case B. The red curve is the settling velocity averaged over the particles, the blue dashed line its time average, while the black dashed line indicates the theoretical terminal velocity.*

approaches 1 and the magnitude of the densities of the phases are different, while for low St_K and $\rho_p/\rho_f \simeq 1$ no enhancement is found.

6.3.2 Force contributions

In order to complete the analysis, the p.d.f.'s of the single to total acceleration ratios are reported in Figs. from 6.3 and 6.4, both for the gravity direction and another one that is said to be "homogeneous".

For case A, plots are very similar to case 2 of the parametric investigation presented in chapter 5, with the Pressure Gradient as the leading term and a non-negligible mean contribution from the Stokes Drag. Indeed, the values of the Stokes number and density ratio are quite similar. No difference between the gravity direction and the other ones is noticed: since these particles are nearly neutrally-buoyant, the effect of gravity is relatively weak.

For case B, the resulting hierarchy of the forces could appear to be surprising. The PG has a smaller, nearly-null mean value, while the viscous forces (SD and

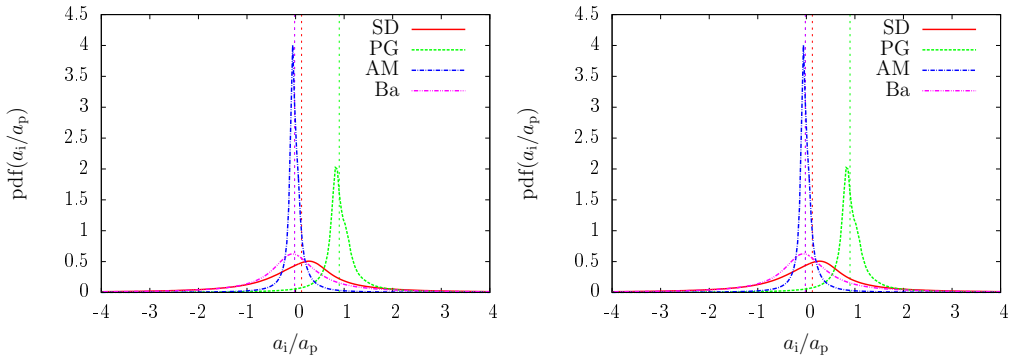

(a) *Case A - Gravity direction* **(b)** *Case A - Homogeneous dir.*

Figure 6.3: *P.d.f.'s of the different acceleration ratios* a_i/a_p *for case A.*

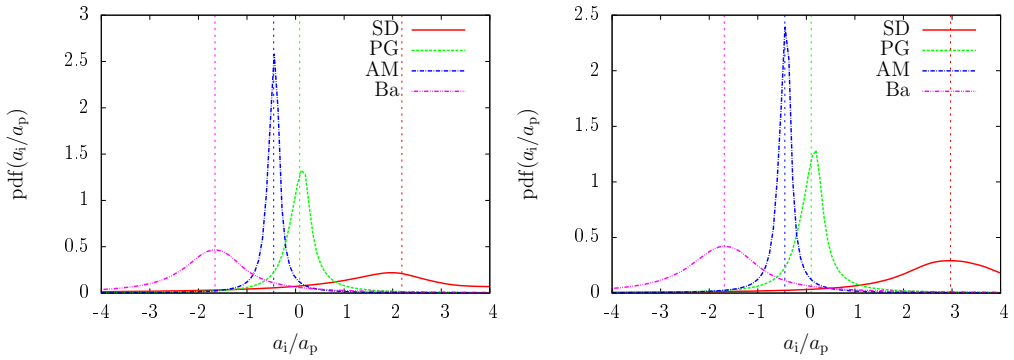

(a) *Case B - Gravity direction* **(b)** *Case B - Homogeneous dir.*

Figure 6.4: *P.d.f.'s of the different acceleration ratios* a_i/a_p *for case B.*

BH) increase considerably. This can be explained with the very small Stokes number: probably we are somehow stressing the model, hence the correct physics could not have been captured.

6.4 Remarks

In this chapter we have investigated the effect of a turbulent flow on the mean settling rate of dispersed particles. We focused on the range of Stokes number and density ratio that is typical of phytoplankton in ocean and performed several simulations. The resulting average settling velocity is compared with the terminal

velocity of the particle in still fluid. For characteristic values of plankton, we do not find a significant variation of the settling rate due to the effect of turbulence, unlike what is known e.g. for heavy particles. Furthermore, the dynamics of plankton-like particles appears to be similar to that of neutrally-buoyant tracers.

Chapter 7

Conclusions

7.1 Final remarks

Through the results from our parametric investigation we wish to present a useful review which is still not completely available at the present time, according to the writer's opinion. We remark that such broad investigation considered all the forces acting on particles by using an appropriate numerical method to compute them. The most general outcome is that the prevailing force acting on particles strongly varies with the particle properties. Indeed, the primary governing parameter is found to be the density ratio. Particles can therefore show very different behaviours, varying from tracers approximating very well fluid elements to highly inertial and clustering particles, with the Stokes number as the essential governing parameter for the formation of clusters.

A very intriguing feature is the role of the Basset History force, that is frequently neglected since it is difficult to deal with. By comparing simulations with and without the BH term, some very interesting results were found, that suggest that this term can be relevant for several reasons.

As a further application, a specific study considering the influence of the turbulent flow on the settling rate of nearly tracer-like particles showed results in accordance with the parametric survey, without any dramatic variation of the settling rate. This investigation aims to give a useful contribution to the field of plankton ecology.

7.2 Future developments

From the observation of the obtained statistical quantities one can note the highly intermittent behaviour of the several acceleration sources. It could be interesting to investigate this aspect for theoretical reasons but also for some deepenings regarding the improvement of flow measurement techniques, which make use of dispersed particles and where a deeper integration between experimental investigation and numerical simulations is relevant. In this regard, the role of the Basset force is a really challenging topic on which many research works are focusing on, since this force appears to be crucial for a correct representation of rare intense events. The effect of BH could help to clarify some of the discrepancies between numerical and experimental results on particle dynamics that are still not fully understood [10].

Concerning the topic of sedimentation, a more complete investigation could improve microorganisms description in shape and other properties. This is on the other hand a promising and developing branch of research activity, featuring e.g. simulations of bacteria behaviours. The application of the dynamical description of the present work to the modelling of biological processes could be a future challenging effort.

Appendix A

Derivation of coefficients for the Basset window evaluation

This appendix shows how the analytical integral in (3.9) is exactly evaluated. Taking out of the integral all the quantities that are constant in each subinterval we obtain:

$$\sum_{n=1}^{N} \int_{\tau_n}^{\tau_{n-1}} \frac{\mathbf{g}_n + (\mathbf{g}_{n-1} - \mathbf{g}_n)(\tau - \tau_n)/\Delta t}{\sqrt{t-\tau}} \, \mathrm{d}\tau = \\ = \sum_{n=1}^{N} \left[\mathbf{g}_n \int_{\tau_n}^{\tau_{n-1}} \frac{1}{\sqrt{t-\tau}} \, \mathrm{d}\tau + \frac{(\mathbf{g}_{n-1} - \mathbf{g}_n)}{\Delta t} \int_{\tau_n}^{\tau_{n-1}} \frac{\tau - \tau_n}{\sqrt{t-\tau}} \, \mathrm{d}\tau \right]$$

Solutions of the resulting integrals are available from literature [29], hence it follows:

$$\sum_{n=1}^{N}\left[\mathbf{g}_n\int_{\tau_n}^{\tau_{n-1}}\frac{1}{\sqrt{t-\tau}}\,\mathrm{d}\tau+\frac{(\mathbf{g}_{n-1}-\mathbf{g}_n)}{\Delta t}\int_{\tau_n}^{\tau_{n-1}}\frac{\tau-\tau_n}{\sqrt{t-\tau}}\,\mathrm{d}\tau\right]=$$

$$=\sum_{n=1}^{N}\left\{\mathbf{g}_n\left[-2\sqrt{t-\tau}\right]_{\tau_n}^{\tau_{n-1}}+\frac{\mathbf{g}_{n-1}-\mathbf{g}_n}{\Delta t}\left[-\frac{2}{3}\sqrt{t-\tau}(-3\tau_n+2t+\tau)\right]_{\tau_n}^{\tau_{n-1}}\right\}=$$

$$=\sum_{n=1}^{N}\left\{2\mathbf{g}_n\left[\sqrt{t-\tau_n}-\sqrt{t-\tau_{n-1}}\right]+\right.$$

$$\left.+\frac{2}{3}\frac{\mathbf{g}_{n-1}-\mathbf{g}_n}{\Delta t}\left[\sqrt{t-\tau_n}(-3\tau_n+2t+\tau_n)-\sqrt{t-\tau_{n-1}}(-3\tau_n+2t+\tau_{n-1})\right]\right\}=$$

$$=\sum_{n=1}^{N}\left\{2\,\mathbf{g}_n\left[\sqrt{n\Delta t}-\sqrt{(n-1)\Delta t}\right]+\right.$$

$$\left.+\frac{2}{3}\frac{\mathbf{g}_{n-1}-\mathbf{g}_n}{\Delta t}\left[\sqrt{n\Delta t}\,2n\Delta t-\sqrt{(n-1)\Delta t}(2n+1)\Delta t\right]\right\}=$$

$$=\sum_{n=1}^{N}\sqrt{\Delta t}\left\{\mathbf{g}_n\left[2\sqrt{n}-2\sqrt{n-1}-\frac{4}{3}n\sqrt{n}+\frac{2}{3}(2n+1)\sqrt{n-1}\right]+\right.$$

$$\left.+\,\mathbf{g}_{n-1}\left[\frac{4}{3}n\sqrt{n}-\frac{2}{3}(2n+1)\sqrt{n-1}\right]\right\}=$$

$$=\frac{4}{3}\,\mathbf{g}_0\sqrt{\Delta t}+\sum_{n=1}^{N-1}\sqrt{\Delta t}\left[\frac{4}{3}(n-1)\sqrt{n-1}-\frac{8}{3}n\sqrt{n}+\frac{4}{3}(n+1)\sqrt{n+1}\right]\mathbf{g}_n+$$

$$+\sqrt{\Delta t}\left[\frac{4}{3}(N-1)\sqrt{N-1}+(2-\frac{4}{3}N)\sqrt{N}\right]\mathbf{g}_N$$

where in the last passage an appropriate switching of the index has been performed in order to have a more suitable form for the implementation.

Appendix B

Laminar Cases

In this appendix we report results from some simple but meaningful tests we performed using the developed code:

1. Falling particle in quiescent fluid: the particle is initially at rest and approaches its terminal velocity, as defined in §6.1.1.

2. Particle with nonzero initial velocity arrested in quiescent fluid. The particle velocity starts from $V(t = 0) = 1$ and approaches zero. Interestingly, the resulting dynamics is symmetric to the previous situation.

We performed the tests for all the cases presented in the parametric investigation of Chapter 5, with and without taking into account the Basset History force. Analytical solutions for these problems are available in literature, and in particular one has been recalled in §3.4.1. In fact, these results also represent a further validation argument since a good accordance between numerical and analytical solutions is always verified (not shown here).

Figs. B.1 and B.2 report the particle velocity time history for the first test, respectively for the case with and without the Basset term. The same is done for the second test with Figs B.3 and B.4. Finally, only for the second test, in Figs from B.5 to B.7 we recollect the plots in order to have a clear sight of the effect of the Basset force. What is found is that this term appears to always delay the transient of the particle velocity i.e. we could affirm that the particle relaxation time is somehow modified by the presence of this force.

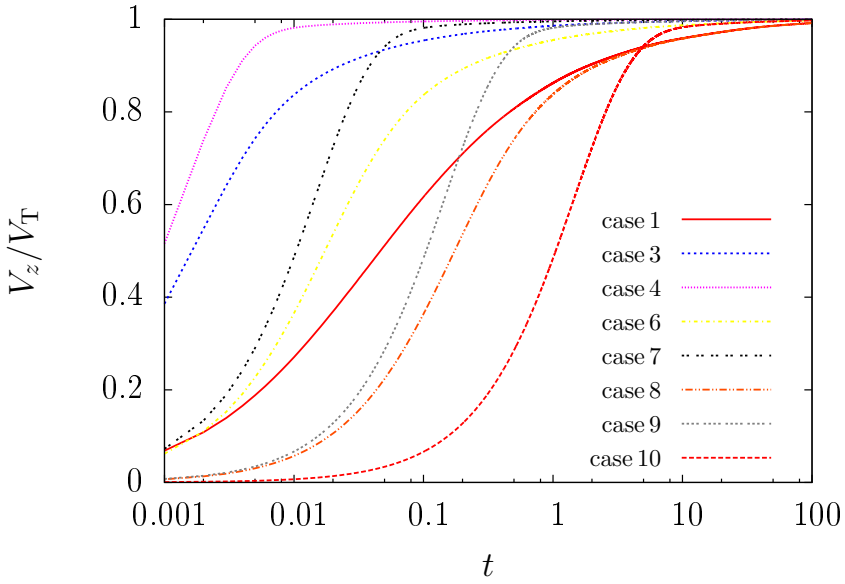

Figure B.1: *Falling particle in quiescent fluid: particle velocity time history, Basset force included.*

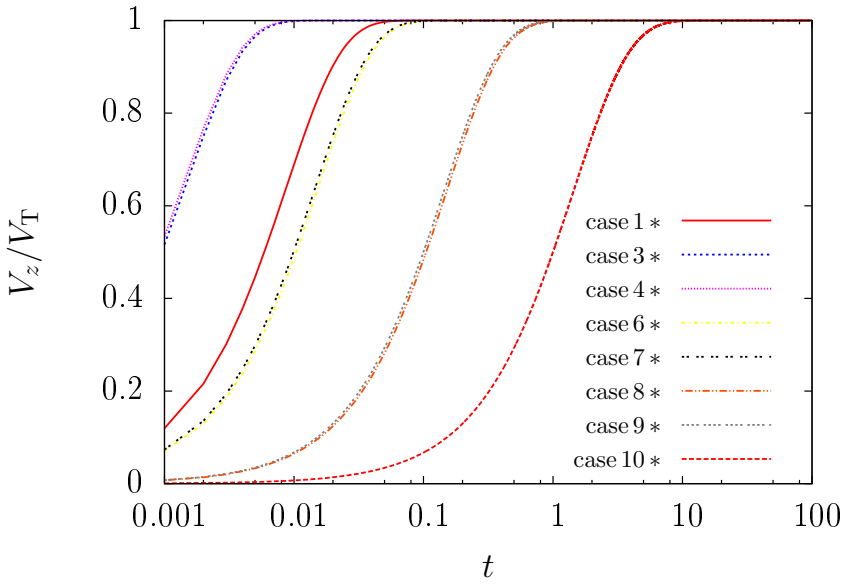

Figure B.2: *Falling particle in quiescent fluid: particle velocity time history, Basset force neglected.*

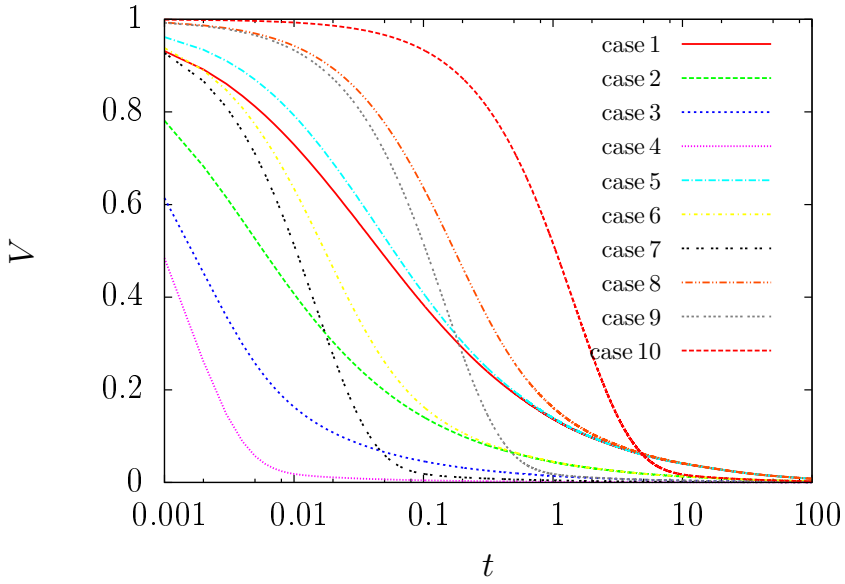

Figure B.3: *Particle arresting in quiescent fluid: particle velocity time history, Basset force included.*

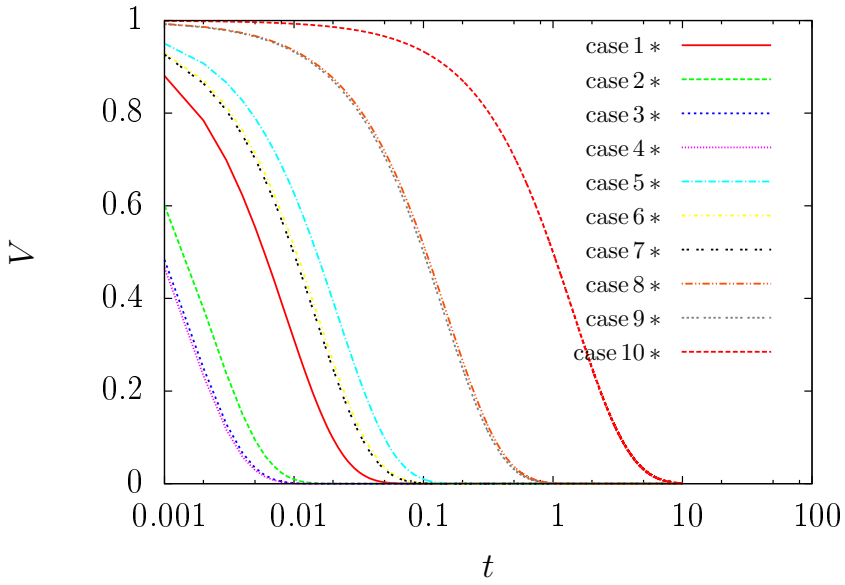

Figure B.4: *Particle arresting in quiescent fluid: particle velocity time history, Basset force neglected.*

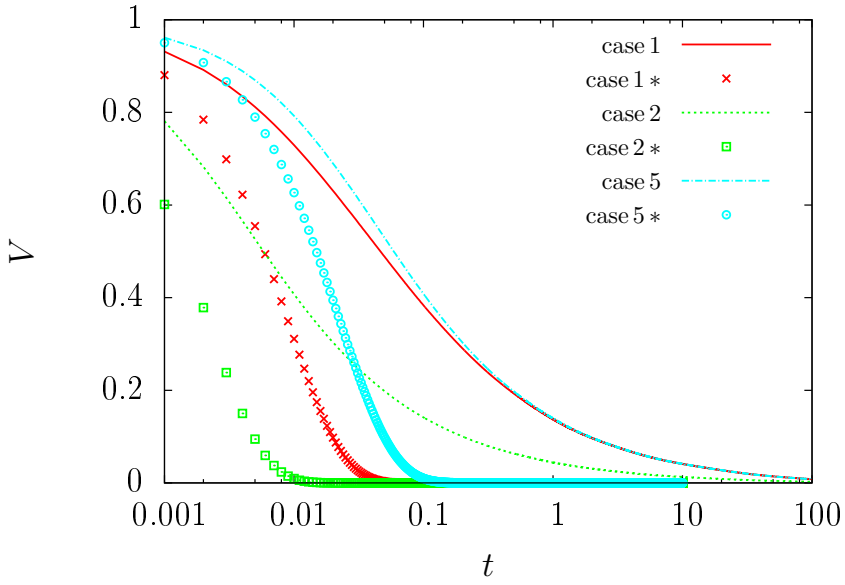

Figure B.5: *Particle arresting in quiescent fluid: comparison between the case with and without the Basset History force for cases with* $R = 0.1, 1$. *Results including the Basset term are displayed by solid lines, results without Basset with symbols.*

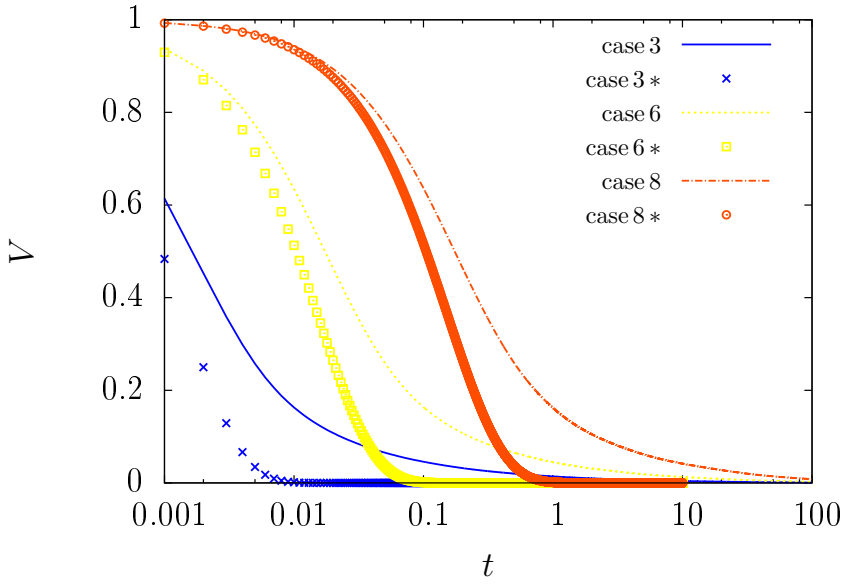

Figure B.6: *Particle arresting in quiescent fluid: comparison between the case with and without the Basset History force for cases with* $R = 10$*. Results including the Basset term are displayed by solid lines, results without Basset with symbols.*

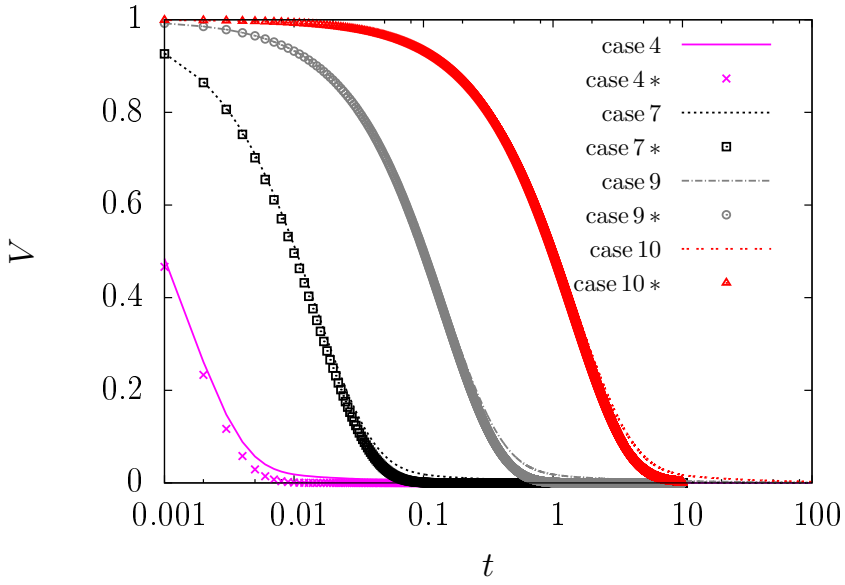

Figure B.7: *Particle arresting in quiescent fluid: comparison between the case with and without the Basset History force for cases with* $R = 1000$*. Results including the Basset term are displayed by solid lines, results without Basset with symbols.*

Appendix C

Acceleration Ratio P.D.F.s of the Parametric Investigation

This appendix reports systematically the probability density function of the acceleration ratio as defined in §4.3.1 for each case of our parametric investigation. In the following pages, the top figure is for the simulation accounting the Basset history force while the bottom one is for the case in which this force has been neglected.

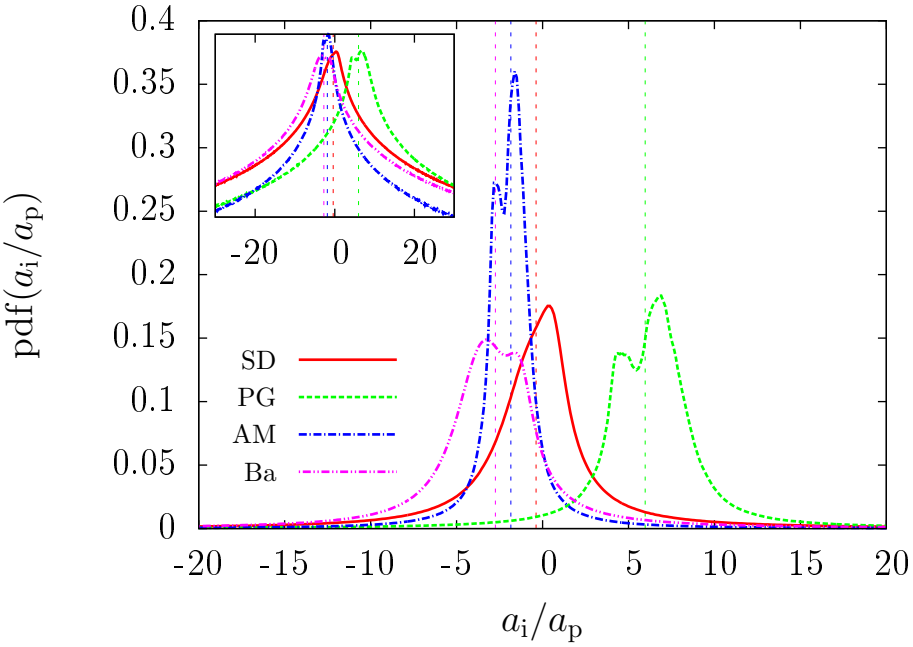

Figure C.1: *Case 1 ($R = 0.1$, $St_\mathrm{K} = 0.01$), Basset force included.*

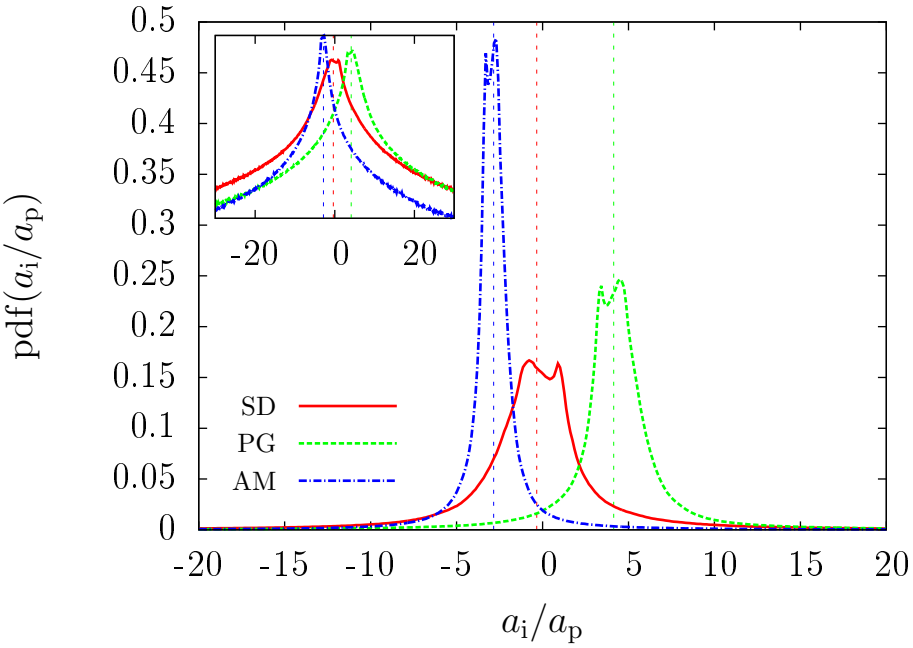

Figure C.2: *Case 1 ($R = 0.1$, $St_\mathrm{K} = 0.01$), Basset force neglected.*

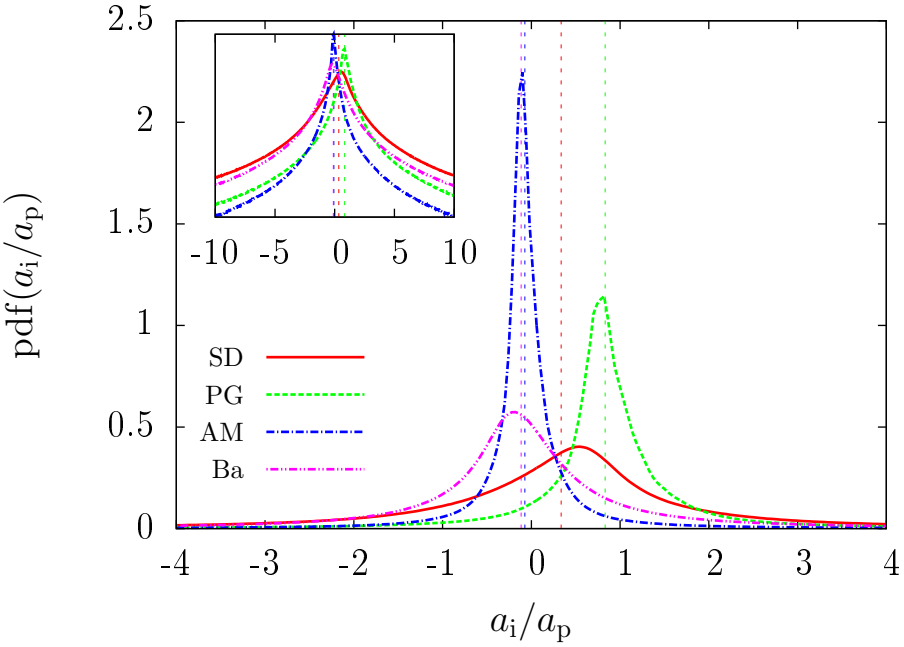

Figure C.3: *Case 2 ($R = 1$, $St_\mathrm{K} = 0.01$), Basset force included.*

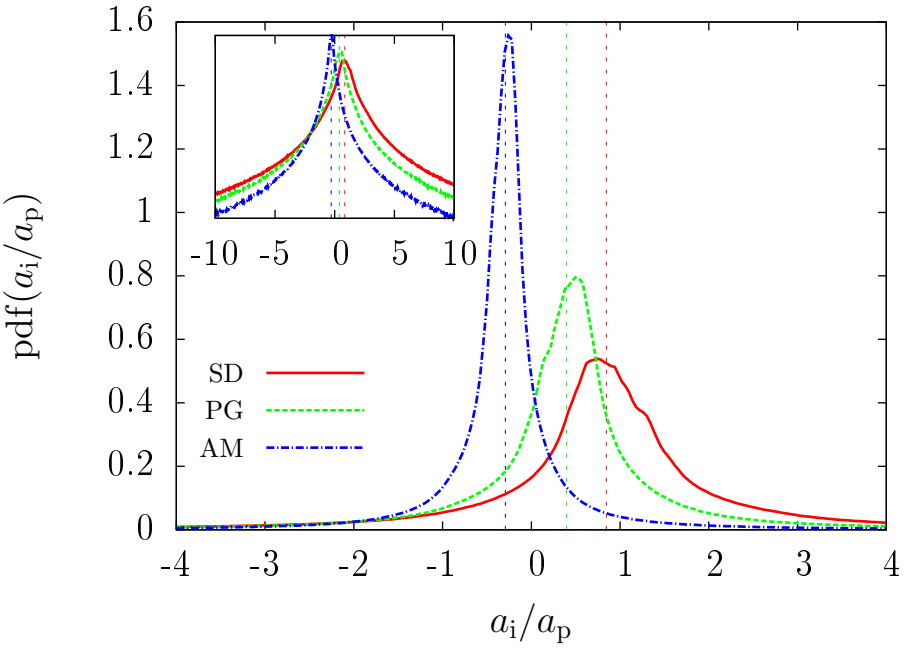

Figure C.4: *Case 2 ($R = 1$, $St_\mathrm{K} = 0.01$), Basset force neglected.*

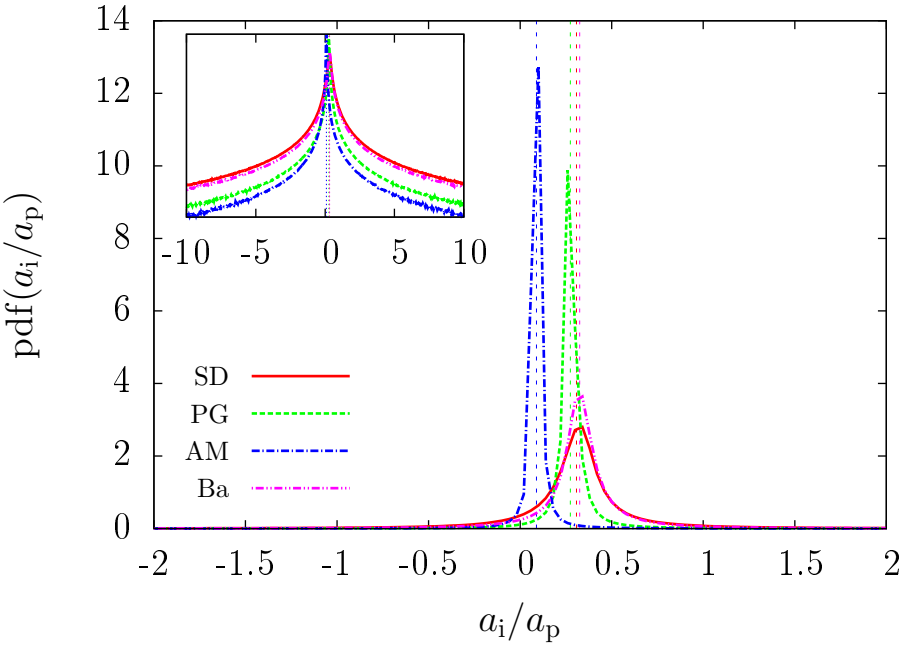

Figure C.5: *Case 3 ($R = 10$, $St_K = 0.01$), Basset force included.*

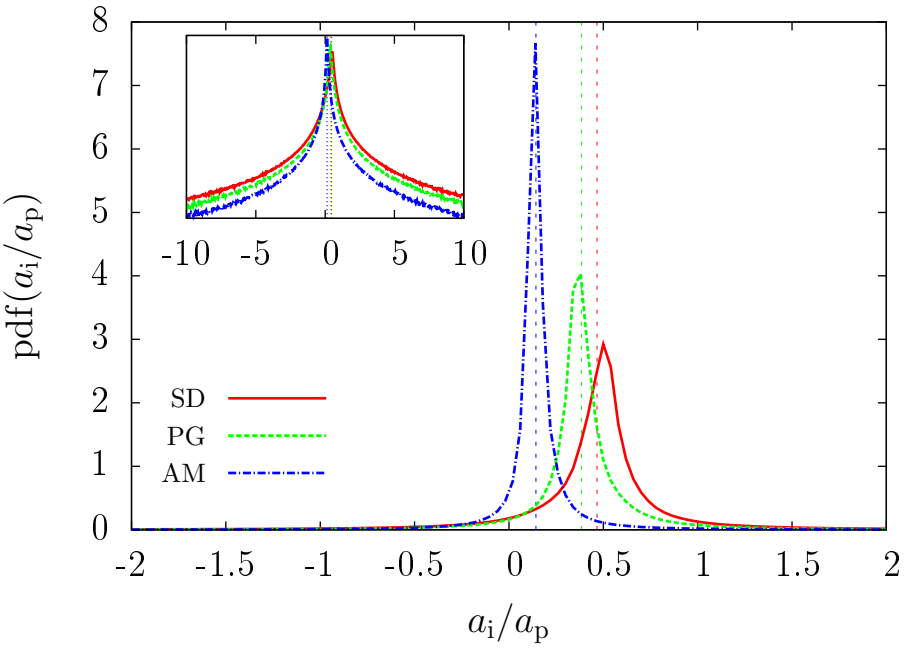

Figure C.6: *Case 3 ($R = 10$, $St_K = 0.01$), Basset force neglected.*

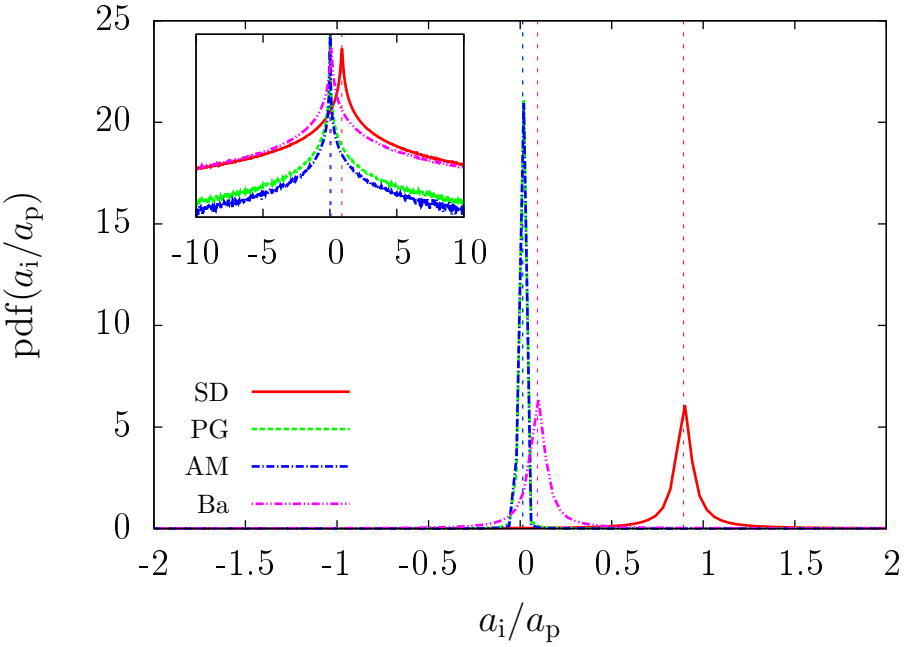

Figure C.7: *Case 4 ($R = 1000$, $St_\mathrm{K} = 0.01$), Basset force included.*

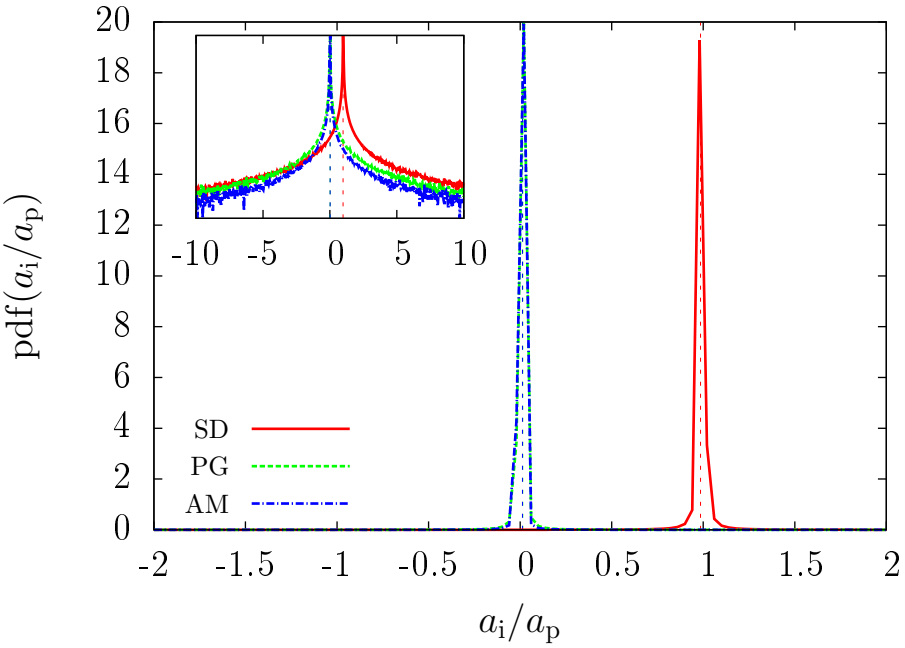

Figure C.8: *Case 4 ($R = 1000$, $St_\mathrm{K} = 0.01$), Basset force neglected.*

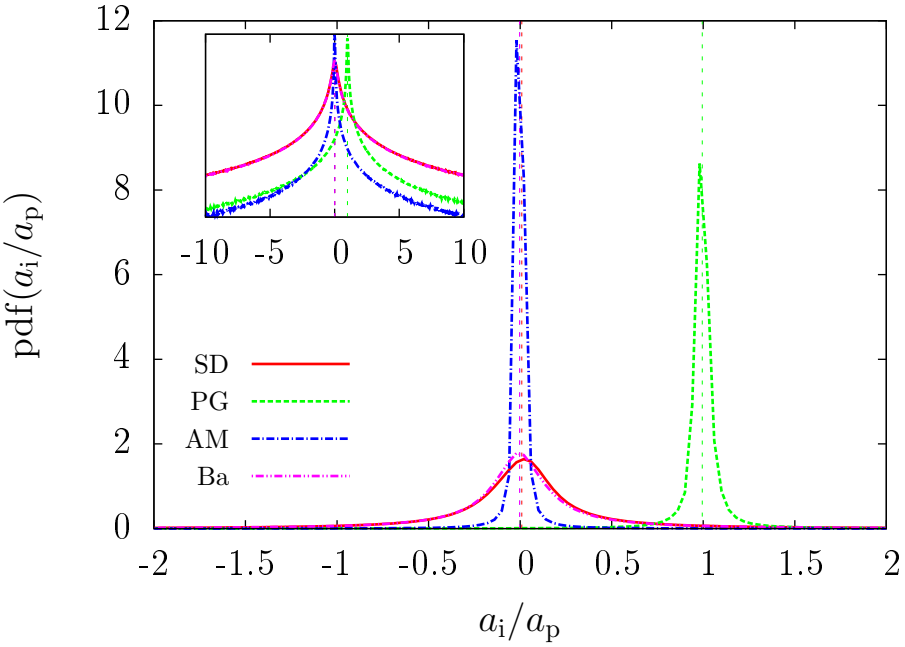

Figure C.9: *Case 5 ($R = 1$, $St_\mathrm{K} = 0.1$), Basset force included.*

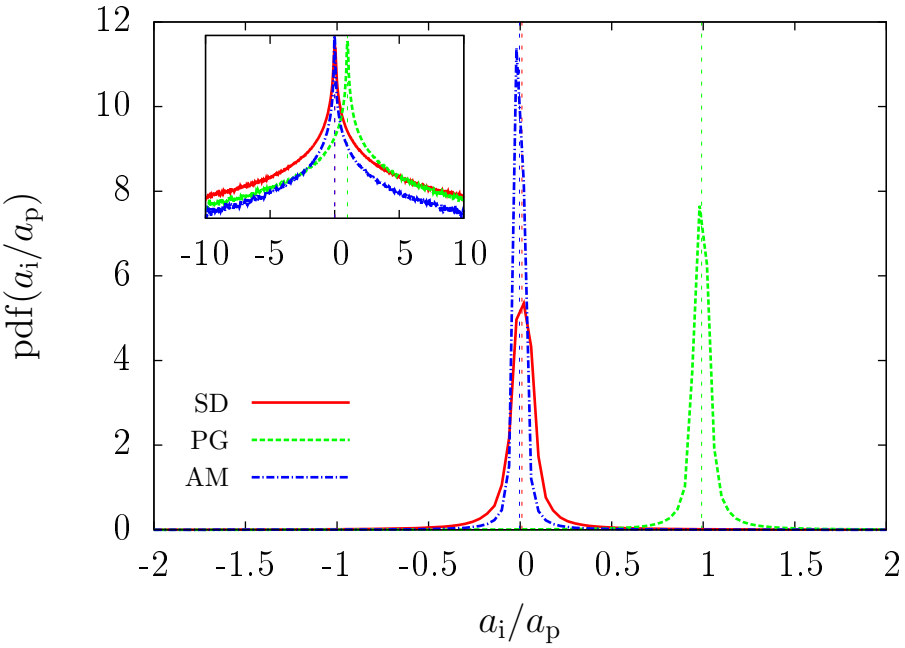

Figure C.10: *Case 5 ($R = 1$, $St_\mathrm{K} = 0.1$), Basset force neglected.*

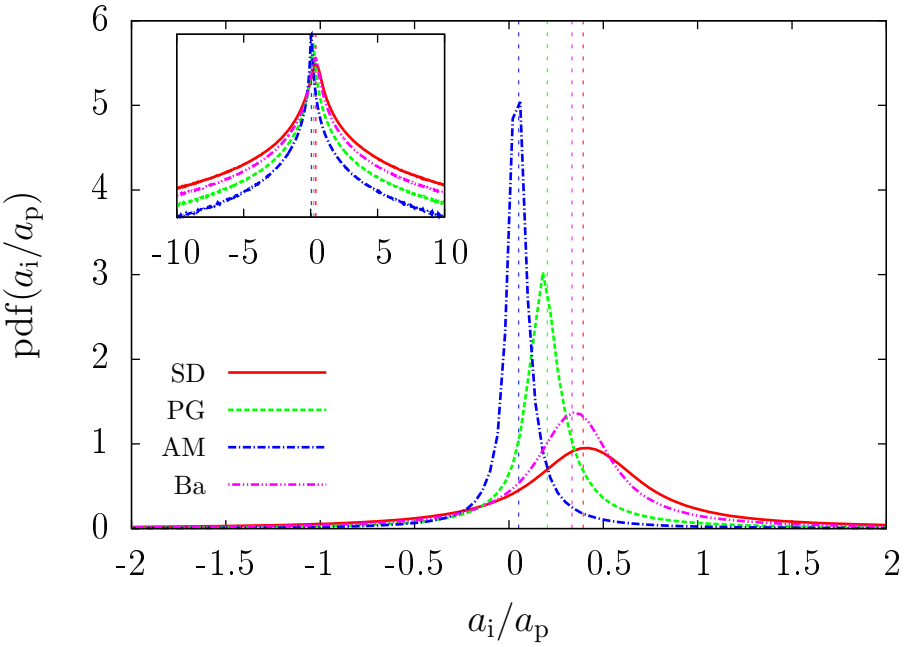

Figure C.11: *Case 6 ($R = 10$, $St_K = 0.1$), Basset force included.*

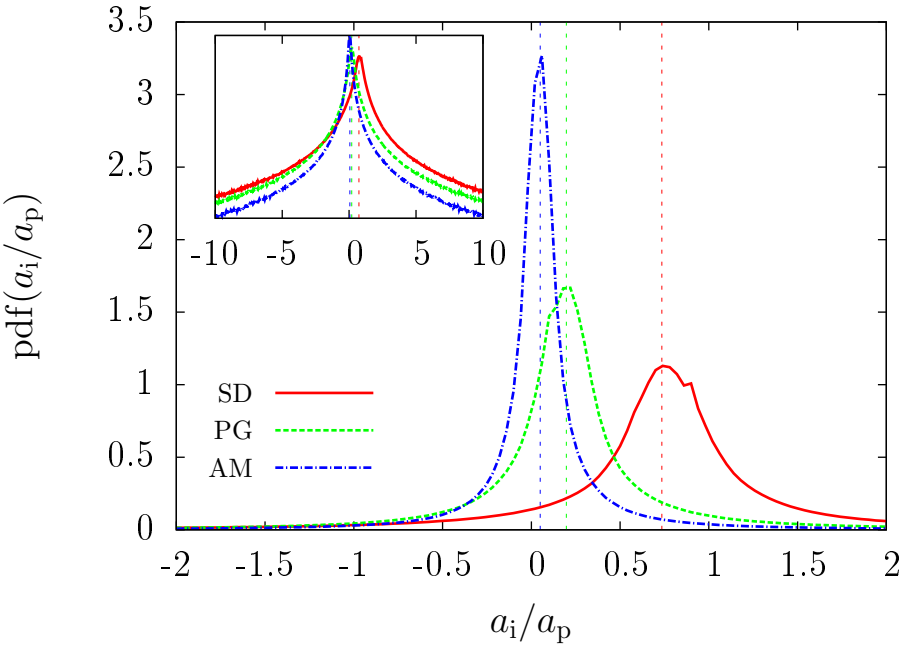

Figure C.12: *Case 6 ($R = 10$, $St_K = 0.1$), Basset force neglected.*

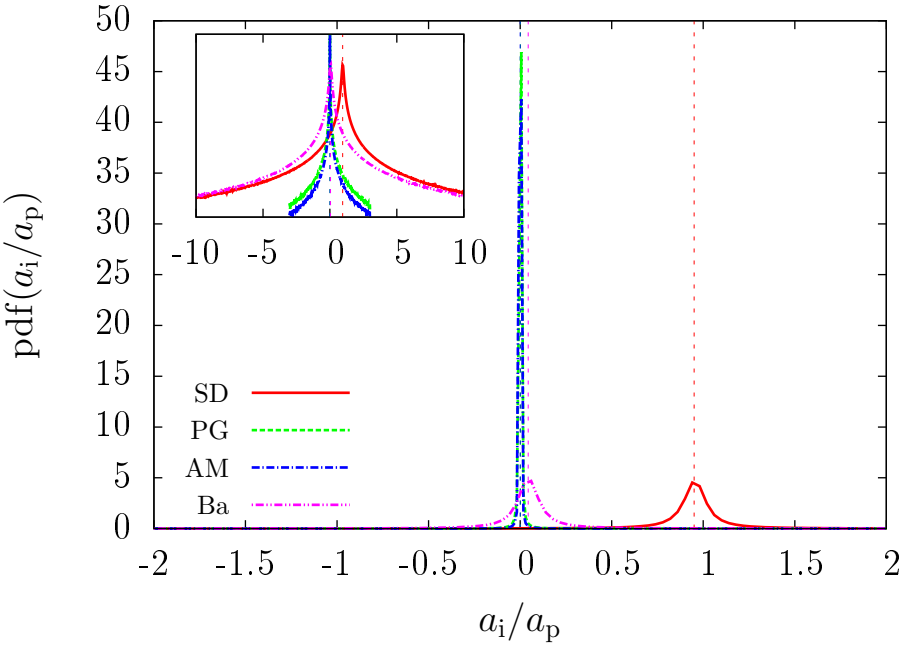

Figure C.13: *Case 7 ($R = 1000$, $St_K = 0.1$), Basset force included.*

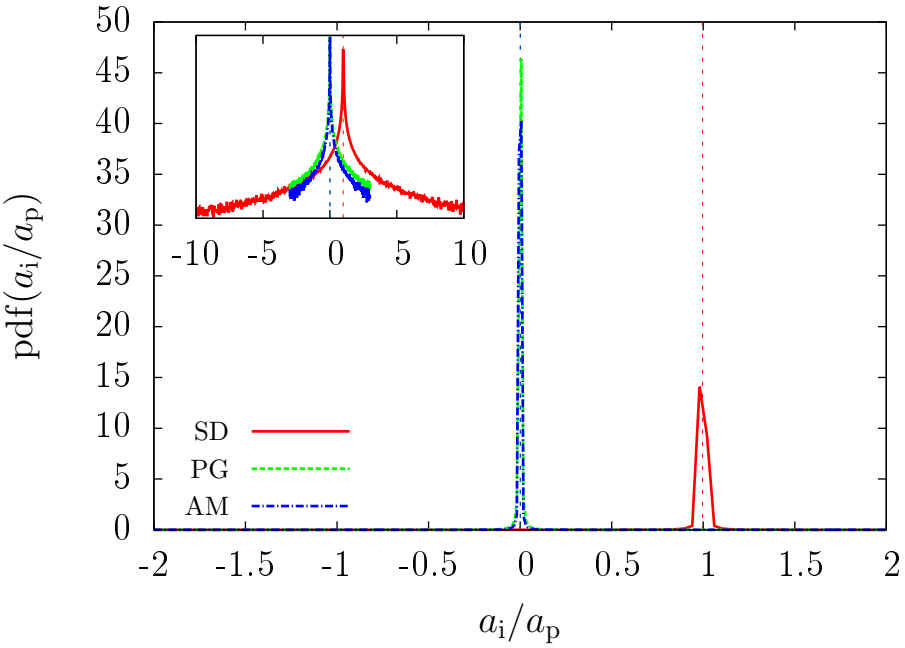

Figure C.14: *Case 7 ($R = 1000$, $St_K = 0.1$), Basset force neglected.*

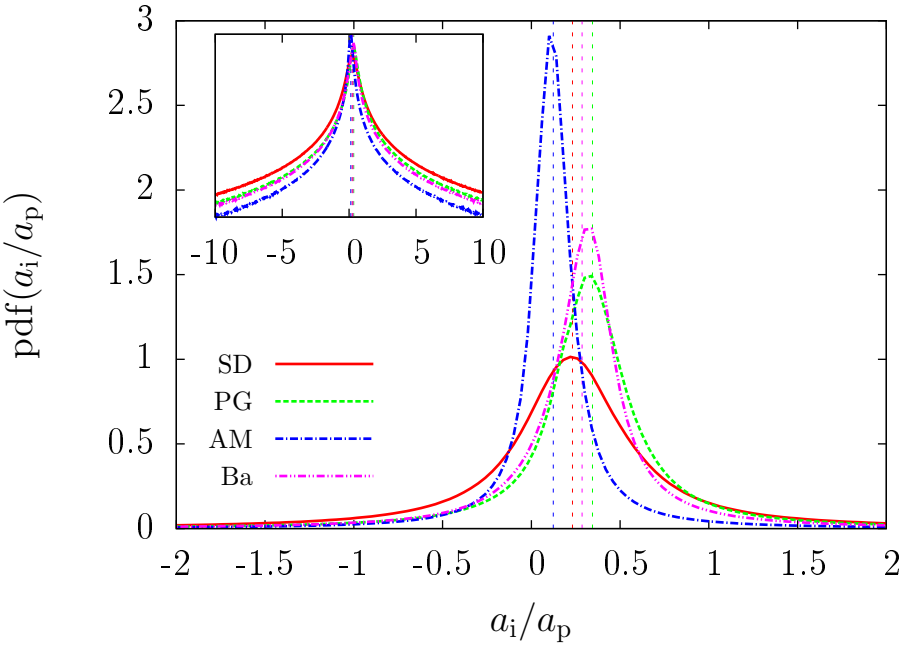

Figure C.15: *Case 8 ($R = 10$, $St_K = 1$), Basset force included.*

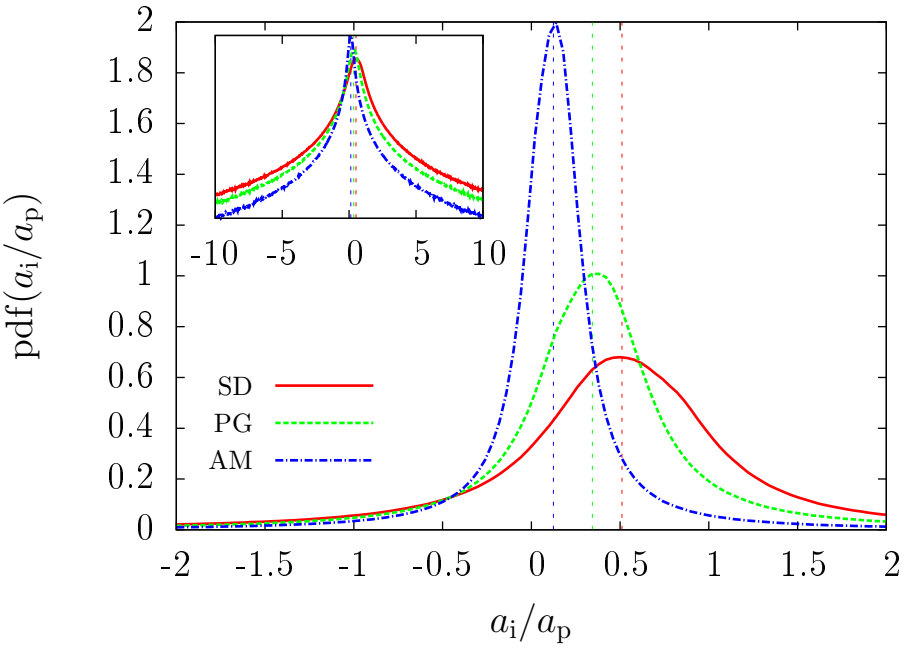

Figure C.16: *Case 8 ($R = 10$, $St_K = 1$), Basset force neglected.*

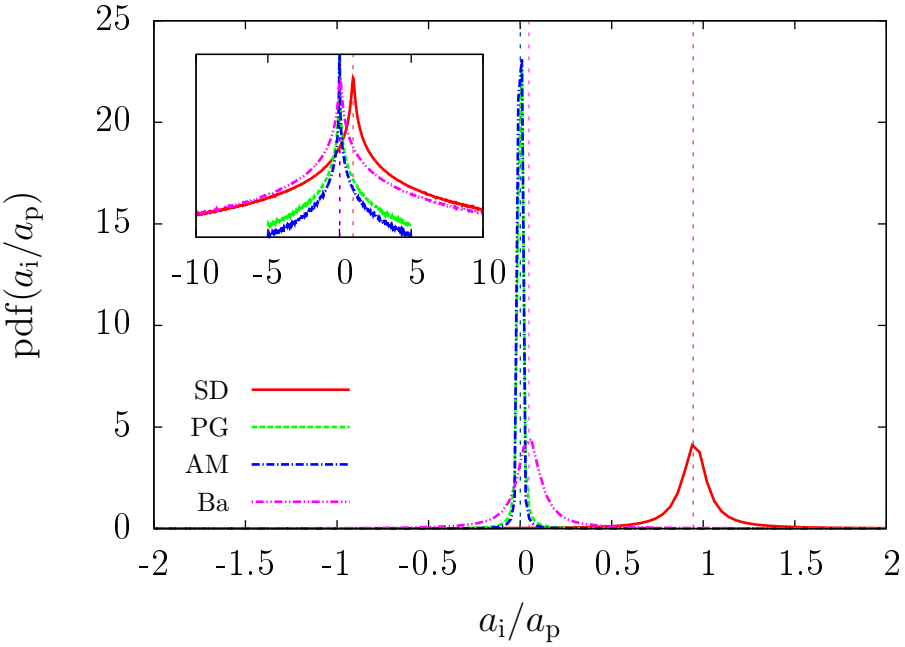

Figure C.17: *Case 9 ($R = 1000$, $St_\mathrm{K} = 1$), Basset force included.*

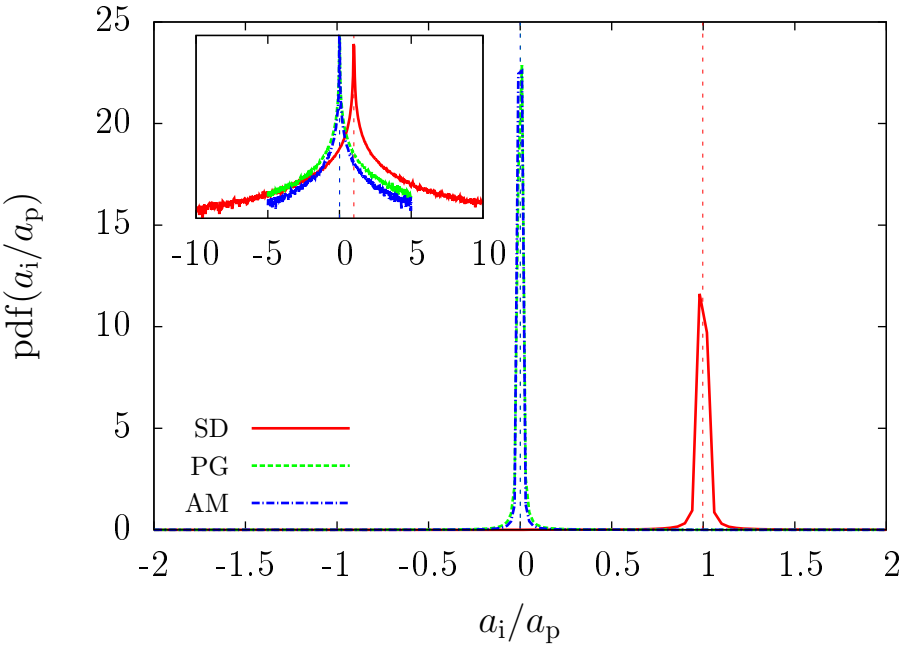

Figure C.18: *Case 9 ($R = 1000$, $St_\mathrm{K} = 1$), Basset force neglected.*

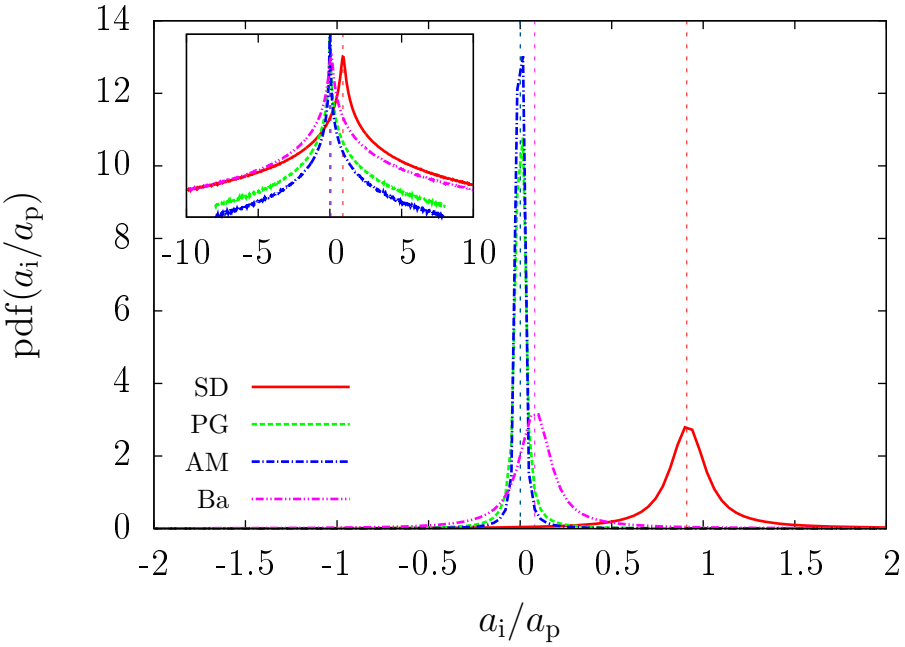

Figure C.19: *Case 10 ($R = 1000$, $St_K = 10$), Basset force included.*

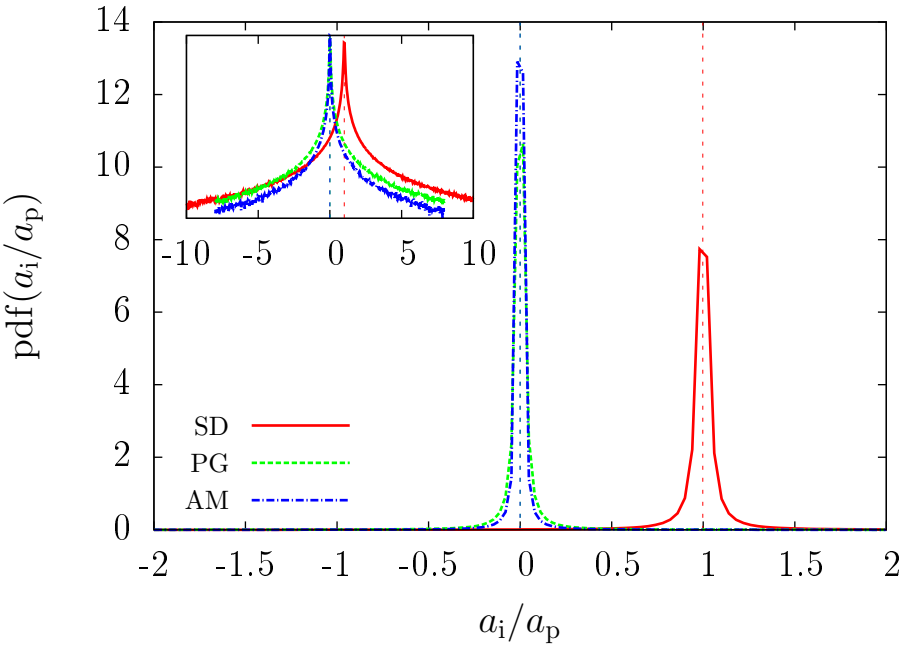

Figure C.20: *Case 10 ($R = 1000$, $St_K = 10$), Basset force neglected.*

Acknowledgements

I am deeply grateful to Prof. Luca Brandt, who warmly received me at his group and supported my work, and Drs. Gaetano Sardina and Francesco Picano for their constant presence, kindness and incentive to research. It was a challenging experience and I really felt part of the team, for which I'm thankful.

My sincere gratitude goes to Prof. Jan Oscar Pralits, for his constant help and closeness. I would like to thank Prof. Alessandro Bottaro for the given opportunity, the trasmitted interest in fluid mechanics and his kind support, and Prof. Andrea Mazzino for the crucial teachings in turbulence and his interest in my work. My grateful thanks are also extended to all the people at DICCA fluid mechanics research group in Genoa, especially Damiano Natali.

I'm very grateful to Foundation Lerici and Italian Cultural Institute in Stockholm for the financial support, an essential help for this experience.

Finally I want to thank all the people I met at Linné FLOW Center: Fabio, Nicolò, Luca, Ugis, Mattias, Taras, Zeinab, George, Ellinor, CJ, Iman, Onofrio, Werner, Enrico, Nima, Armin, Azad... TACK!

Il traguardo finalmente raggiunto non sarebbe stato possibile senza il supporto costante e totale da parte della mia famiglia, l'aiuto dei compagni di studio e la vicinanza dei tanti amici. A tutti il mio più sentito Grazie dal profondo del cuore.

Genova, Dicembre 2013 S. O.

Bibliography

[1] M. van Aartrijk and H. J. H. Clercx. “Dispersion of (Light) Inertial Particles in Stratified Turbulence”. In: ERCOFTAC Series 13 (2010). Ed. by Vincenzo Armenio, Bernard Geurts, and Jochen Fröhlich, pp. 457–463.

[2] M. van Aartrijk and H. J. H. Clercx. “Vertical dispersion of light inertial particles in stably stratified turbulence: The influence of the Basset force”. In: *Physics of Fluids* 22.1, 013301 (2010), p. 013301.

[3] R. J. Adrian. “Particle-Imaging Techniques for Experimental Fluid-Mechanics”. In: *Annual Review of Fluid Mechanics* 23 (1991), pp. 261–304.

[4] V. Armenio and V. Fiorotto. “The importance of the forces acting on particles in turbulent flows”. In: *Physics of Fluids* 13.8 (2001), pp. 2437–2440.

[5] T. R. Auton, J. C. R. Hunt, and M. Prud’Homme. “The force exerted on a body in inviscid unsteady non-uniform rotational flow”. In: *Journal of Fluid Mechanics* 197 (1988), pp. 241–257.

[6] S. Balachandar and J. K. Eaton. “Turbulent Dispersed Multiphase Flow”. In: *Annual Review of Fluid Mechanics* 42.1 (2010), pp. 111–133.

[7] A. B. Basset. *A treatise on Hydrodynamics. Vol. 2*. Dover publications, 1961.

[8] G. K. Batchelor. *An Introduction to Fluid Dynamics*. Cambridge Mathematical Library. Cambridge University Press, 2000.

[9] J. V. Boussinesq. *Theorie Analytique de la Chaleur. Vol. 2*. L’École Polytechnique, 1903.

[10] E. Calzavarini et al. “Acceleration statistics of finite-sized particles in turbulent flow: the role of Faxén forces”. In: *Journal of Fluid Mechanics* 630 (2009), p. 179.

[11] S. Corrsin and J. Lumley. “On the equation of motion for a particle in turbulent fluid”. In: *Applied Scientific Research* 6 (2 1956), pp. 114–116.

[12] A. Daitche and T. Tél. “Memory Effects are Relevant for Chaotic Advection of Inertial Particles”. In: *Phys. Rev. Lett.* 107 (24 2011), p. 244501.

[13] S. Elghobashi and G. C. Truesdell. “Direct simulation of particle dispersion in a decaying isotropic turbulence”. In: *Journal of Fluid Mechanics* 242 (), pp. 655–700.

[14] P. D. Friedman and J. Katz. “Mean rise rate of droplets in isotropic turbulence”. In: *Physics of Fluids* 14.9 (2002), pp. 3059–3073.

[15] U. Frisch and A. A. N. Kolmogorov. *Turbulence: The Legacy of A. N. Kolmogorov*. Cambridge University Press, 1995.

[16] M. A. T. van Hinsberg, J. H. M. Thije Boonkkamp, and H. J. H. Clercx. “An efficient, second order method for the approximation of the Basset history force”. In: *Journal of Computational Physics* 230 (2011), pp. 1465–1478.

[17] J. Jacobsen, A. Jayaraman, and A. Belmonte. “Monotone Solutions of a Nonautonomous Differential Equation for a Sedimenting Sphere”. In: *ArXiv Mathematical Physics e-prints* (Dec. 2000).

[18] P. K. Kundu and I. M. Cohen. *Fluid Mechanics*. Academic Press. Academic Press, 2010.

[19] R. LeVeque. *Finite Difference Methods for Ordinary and Partial Differential Equations: Steady-State and Time-dependent Problems*. Society for Industrial and Applied Mathematics, 2007.

[20] E. Loth. “Numerical approaches for motion of dispersed particles, droplets and bubbles”. In: *Progress in Energy and Combustion Science* 26.3 (2000), pp. 161 –223.

[21] M. R. Maxey. “The gravitational settling of aerosol particles in homogeneous turbulence and random flow fields”. In: *Journal of Fluid Mechanics* 174 (), pp. 441–465.

[22] M. R. Maxey and S. Corrsin. “Gravitational Settling of Aerosol Particles in Randomly Oriented Cellular Flow Fields.” In: *Journal of Atmospheric Sciences* 43 (1986), pp. 1112–1134.

[23] M. R. Maxey and J. J. Riley. “Equation of motion for a small rigid sphere in a nonuniform flow”. In: *Physics of Fluids* 26.4 (1983), pp. 883–889.

[24] R. Mei, R. J. Adrian, and T. J. Hanratty. “Particle dispersion in isotropic turbulence under Stokes drag and Basset force with gravitational settling”. In: *Journal of Fluid Mechanics* 225 (1991), pp. 481–495.

[25] E. E. Michaelides. *Particles, Bubbles & Drops: Their Motion, Heat And Mass Transfer*. World Scientific, 2006.

[26] C. W. Oseen. *Hydrodynamik*. Leipzig, 1927.

[27] S. B. Pope. *Turbulent flows*. Cambridge University Press, 2000.

[28] J. C. Prairie et al. “Biophysical interactions in the plankton: A cross-scale review”. In: *Limnology & Oceanography: Fluids & Environments* 2 (2012), pp. 121–145.

[29] L. Rade and B. Westergren. *Mathematics Handbook for Science and Engineering*. Springer, 2010.

[30] M. W. Reeks. “On the dispersion of small particles suspended in an isotropic turbulent fluid”. In: *Journal of Fluid Mechanics* 83 (03), pp. 529–546.

[31] M. W. Reeks and S. McKee. “The dispersive effects of Basset history forces on particle motion in a turbulent flow”. In: *Physics of Fluids* 27.7 (1984), pp. 1573–1582.

[32] C. S. Reynolds. *The Ecology of Phytoplankton*. Ecology, Biodiversity, and Conservation. Cambridge University Press, 2006.

[33] J. J. Riley. “PhD Thesis”. PhD thesis. The Johns Hopkins University, 1971.

[34] J. Ruiz, D. Macías, and F. Peters. “Turbulence increases the average settling velocity of phytoplankton cells”. In: *Proceedings of the National Academy of Sciences of the United States of America* 101.51 (2004), pp. 17720–17724.

[35] W. H. Snyder and J. L. Lumley. “Some measurements of particle velocity autocorrelation functions in a turbulent flow”. In: *Journal of Fluid Mechanics* 48 (01), pp. 41–71.

[36] K. D. Squires and J. K. Eaton. “Preferential concentration of particles by turbulence”. In: *Physics of Fluids* 3.5 (1991), pp. 1169–1178.

[37] C. M. Tchen. “Mean value and correlation problems connected with the motion of small particles suspended in a turbulent fluid”. PhD thesis. TU Delft, Delft University of Technology, 1947.

[38] F. Toschi and E. Bodenschatz. “Lagrangian Properties of Particles in Turbulence”. In: *Annual Review of Fluid Mechanics* 41 (2009), pp. 375–404.

[39] L.-P. Wang and M. R. Maxey. “Settling velocity and concentration distribution of heavy particles in homogeneous isotropic turbulence”. In: *Journal of Fluid Mechanics* 256 (1993), pp. 27–68.

[40] T. S. Yang and S. S. Shy. “The settling velocity of heavy particles in an aqueous near-isotropic turbulence”. In: *Physics of Fluids* 15.4 (2003), pp. 868–880.